2

Improvement of Microarray Technologies for Detecting Single Nucleotide Mismatch

HONG WANG, ZUHONG LU*, JIONG LI, HEPING LIU, AND QUANJUN LIU
Chien-Shiung Wu Laboratory, Department of Biomedical Engineering, Southeast University, Nanjing, China 210096

Abstract: With the completion of the Human Genome Project and beginning of post genome era, there is an urgent need for a fast, specific, sensitive, reliable and cost-effective method for the genome-wide polymorphism analysis. Microarray technology is one of the most promising approaches to this need. There are two major concerns in the microarray technology; one is target labeling and the other is the reliability of single nucleotide mismatch discrimination. In this chapter, we reported our recent progress in molecular beacon arrays for detecting label-free targets and a microarray based melting-curve analysis method for improving the reliability of single nucleotide mismatch discrimination. Several successful practical applications of these improved microarray technologies have also been illustrated.

Key words: Microarray, SNPs, mutations, molecular beacon, melting-curve analysis.

1. Introduction

The past few years have witnessed an extraordinary surge of interest in the microarray technology(1-3). A microarray is a collection of miniaturized test sites fabricated on a solid substrate either by robotically spotting or by *in situ* synthesizing with photo-deprotection method, inkjet spraying method or molecular stamping method(4-7). It permits many tests to be performed in a parallel and high-throughput way and offers the first great hope for 'global views' of DNA and RNA variation during biological processes instead of the traditional gene–by–gene approach.

The application of the microarray technology in monitoring RNA expression levels of thousands of genes was well established and widely reported (8-9). But other applications, such as identification and genotyping of point mutations and single nucleotide polymorphisms (SNPs), are still in their infant stage and many issues remain to be worked out.

SNPs are most commonly occurred variant, and are estimated to be 1 out of every 1000 bases in the human genome (10). With the completion of the Human Genome Project and beginning of post genome era, more and more SNPs and point mutations are being uncovered and assembled into large SNP databases. The large number of SNPs provides a rich set of markers that can be used in a wide variety of genetic studies. The identification of a complex set of genes that cause a disease also requires both linkage and association analyses of thousands of SNPs across the human genome in thousands of individuals.

Since the important roles of SNPs and point mutations in molecular biology, many assay principles have been developed in the last 20 years (11-12). Even most of these principles were firstly illustrated in homogeneous solution; many efforts have been devoted to implement them in a microarray assay format to meet the urgent needs for a fast, specific, sensitive, reliable and cost-effective method for a genome-wide SNPs analysis. For example, the allele specific oligonucleotide hybridization is employed in most of the microarray based SNPs genotyping methods, such as the Genechip assay provided by Affymetrix. Other examples are microarray based single nucleotide primer extension reactions, oligonucleotide ligation reactions and enzymatic cleavage methods which provide a better power of discrimination between genotypes than allele specific oligonucleotides hybridizations.

Microarray technology is one of the most promising approaches for large scale and high throughput genotyping. There are two major concerns in the microarray technology; first is the target labeling. Labeling is an important step in most of the microarray based target preparing protocol. It is not only time consuming, and rather expensive, but can also change the levels of targets originally present in the sample. Some label free techniques used in biosensors, such as QCM, SPR and RIfS are not compatible with high throughput applications and lack sensitivity in low molecular weight DNA detection. Second is the reliability of single nucleotide mismatch discrimination. The melting curve of the immobilized duplex is greatly broadened and depressed which greatly reduces the fluorescence intensity difference between the perfect matched duplex and the single base mismatched one. Moreover, it is difficult to normalize the hybridization conditions for a microarray because of massive number of probes and the insufficient knowledge of hybridization reactions at the solid-liquid interface

In this chapter, we reported our recent progress in resolving the above problems. First, a molecular beacon array was constructed, which allowed one to work with unlabelled targets and to retain the high sensitivity of fluorescence techniques. Second, a microarray based melting curve analysis method was investigated. Several successful practical applications of these improved microarray technologies were also illustrated.

2. Molecular Beacon Arrays

2.1 Molecular Beacons

Molecular beacons are oligonucleotide probes that can report the presence of specific nucleic acids in homogeneous solutions (13). They are single-stranded oligonucleotides containing a loop sequence complementary to the target that is flanked by a self-complementary stem, which carries a fluorophore on one end and a quencher at the other end. In the absence of target, the self-complementary stem structure holds the fluorophore so close to the quencher that fluorescence does not occur. When binding to the target, the rigidity of the probe–target duplex forces the stem to unwind, causing the separation of the fluorophore and the quencher and the restoration of fluorescence (Figure 2.1).

Molecular beacons are useful in situations where it is either not possible or desirable to isolate the probe-target hybrids from an excess of the hybridization probes, such as in real-time monitoring of polymerase chain reactions in sealed tubes or for the detection of RNAs within living cells. Therefore, they have been widely used in detecting SNPs and mutations (14-15), virus and pathogens (16-17), amplicons generated in nucleic acid sequence based amplification (NASBA) (18), mRNA in *in vivo* applications (19), and single strand DNA binding protein (20).

Since the first report of molecular beacons in 1996, several improvements and new developments of the molecular beacon technology have been reported. Multicolored molecular beacons (21) were firstly used for allele genotyping in the same solution and they displayed excellent specificity for single nucleotide mismatch discrimination. They had also been used in detecting four different retroviruses. The high sensitivity and specificity of

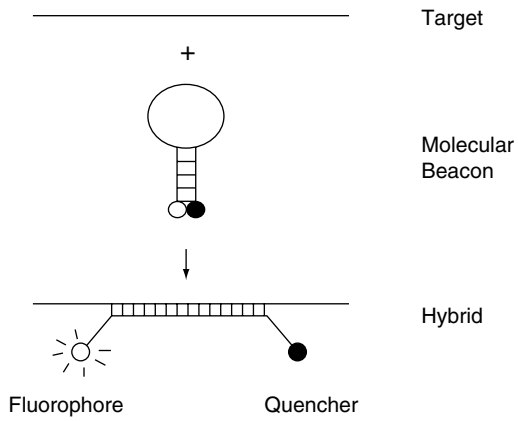

FIGURE 2.1. Scheme of molecular beacon.

each color reaction allowed the detection of fewer than ten copies of one virus amidst a background of unrelated viruses. To overcome the low excitation efficiency of multicolor molecular beacon by monochromatic light source provided by most of the commercialized instrument (such as PCR instrument, fluorescence microscopy, etc.), the wavelength-shifting molecular beacon was introduced (22). Using a combination of conventional molecular beacons and wavelength-shifting molecular beacons it will be possible to reliably perform six-plex or seven-plex PCRs simultaneously.

In another approach, the incorporation of the gold nanoparticles as a quencher instead of the commonly used (DABCYL) substantially increased the sensitivity and specificity of the assay because of the superior quenching ability of gold clusters (23). Moreover, the quenching ability of gold is not limited to its use in clusters. It is possible to construct a molecular beacon array on a gold surface and use the surface as a quencher of fluorescence.

Even many efforts were devoted to construct a serial of molecular beacons to resolve multiplex target simultaneously, the number of the targets was strictly limited due to the limitation of the suitable fluorescent labels. Recently, several groups intended to immobilize molecular beacons onto a solid surface and construct a molecular beacon array to resolve the target DNA sequences spatially.

Tan et al. firstly immobilized a set of molecular beacons on a silica surface through biotin-avidin binding to construct a micrometer DNA biosensor (24-25). They achieved the rapid response, stable, and reproducible results by such kind of DNA biosensors, which make it possible to detect a large number of targets simultaneously. Brown et al. synthesis molecular beacon attached to long chain alkyl amino-controlled pore glass (LCAA-CPG) (26). It can hybridize the target DNA or RNA and restore fluorescence that can be isolated and analyzed. Steemers et al. immobilized molecular beacons on a randomly ordered optic fiber to construct gene arrays (27). They greatly decreased the feature size to construct a miniaturized array capable of detecting unlabeled DNA targets at subnanomolar concentrations. Taking the advantages of low diffusion limitations and high local concentrations of sensing beads on the distal end of fiber, they improved the signal-to-background ratio. The above works opened up an important area of label-free large-scale and high-throughout detection of DNA sequence information.

However, there are still several bottlenecks unsolved for the molecular beacon array technology in practical applications. The electrostatic properties at the solid-liquid interface and the local ion strength of the immobilized molecular beacons are greatly different from that in the bulk solution. The stem structure of the molecular beacon is greatly destabilized which causes high fluorescent background and greatly decreases the signal-background ratio. Presently, the fluorescence increment ratio of the complementary immobilized molecular beacon probes to that of the noncomplementary ones is just about 1-2 after hybridization with targets, while this ratio of the same molecular beacons is tens to hundreds in homogeneous solutions.

Our group tried to improve the molecular beacon immobilization technique. We chose different modified substrates for immobilizing molecular beacons and investigated the annealing and hybridization properties of the molecular beacon arrays immobilized on different substrates (28).

2.2 Fabrication of Molecular Beacon Arrays

2.2.1 The Design of Molecular Beacons for Immobilization

To investigate the hybridization properties of immobilized molecular beacons and potential for constructing molecular beacon array for label-free target detection, we carefully designed amino-modified molecular beacon probes.

The molecular beacons designed for immobilization contain three parts (Figure 2.2): First, a single strand hairpin structure. Most studies have indicated that 15 to 25 base loop together with 5 to 7 base pair stem will provide an appropriate balance to form a hairpin structure, we choose a 16 base loop and 6 base pair stem in our design. Five molecular beacon probes were carefully

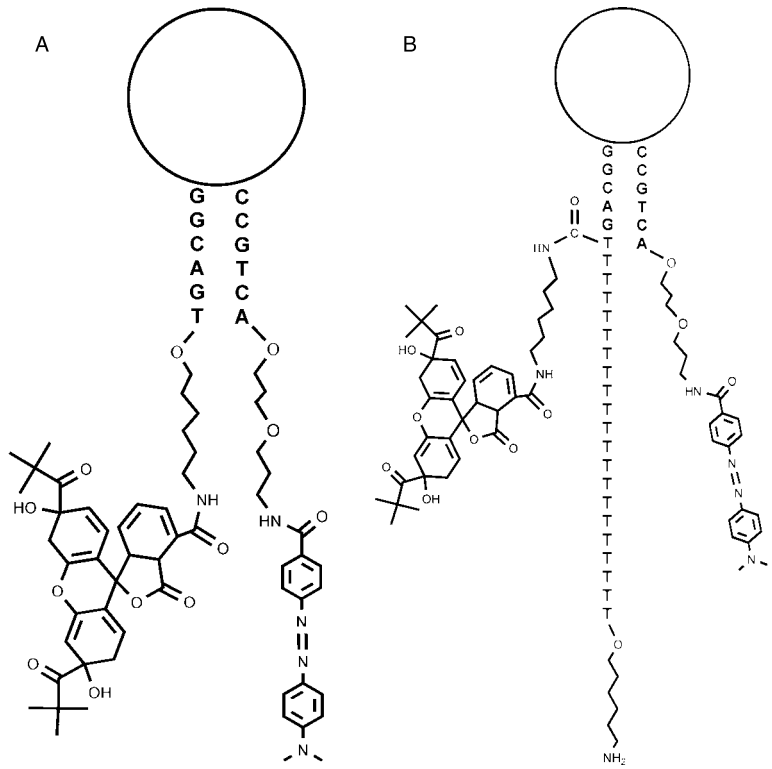

FIGURE 2.2. Structure of (A) molecular beacon and (B) amino modified molecular beacon for immobilization.

TABLE 2.1. Molecular beacon probe and target sequences

Symbol	Sequence
MB1	NH2-(T)20-FAM-TGACGG GAAGGTGGAATGGTTG CCGTCA-DABCYL
MB2	NH2-(T)20-FAM-TGACGG TGCAGAAG**C**GCCTGGC CCGTCA-DABCYL
MB3	NH2-(T)20-FAM-TGACGG TGCAGAAG**T**GCCTGGC CCGTCA-DABCYL
MB4	NH2-(T)20-FAM-TGACGG TGCAGAAG**G**GCCTGGC CCGTCA-DABCYL
MB5	NH2-(T)20-FAM-TGACGG TGCAGAAG**A**GCCTGGC CCGTCA-DABCYL
T2	GCCAGGC**G**CTTCTGCA
T3	GCCAGGC**A**CTTCTGCA

Note: Underline indicates the stem sequence of molecular beacon. Bold underline indicates the single nucleotide difference between sequences.

selected: four of them (MB2-MB5) targets an allele of human apoE gene and have one base difference at the central position of loop sequences. They are used to demonstrate the single nucleotide discrimination capability. MB1 is used as negative control and has a non-related loop sequence with MB2-MB5. All molecular beacon probes and corresponding target sequences are listed in Table 2.1. Second, a fluorescein in the internal location within the 5′ arm is used as the fluorophore and a 3′-end [4-(4-dimethylaminopherylazo) benzoic acid] (DABCYL) is used as the quencher. Fluorescein and DABCYL are most widely used fluorophore and quencher pair because DABCLY are nonfluorescent and can quench the fluorescein extremely well. Third, a 20 base thymine spacer with an amino group linked to 5′ end extends past the position of the fluorescein on the 5′ arm of our molecular beacons. The 20-base-thymine is used to increase the flexibility of molecular beacon and to minimize destabilization effects caused by 5′-end immobilization. The 5′ end amino-modified molecular beacon probes can be covalently immobilized on the activated substrates via the Schiff base aldehyde-amine chemistry.

The hybridization results in solution indicate the spacer structure of the molecular beacons for immobilization will decrease the quench efficiency, but the effects can be neglected and the probes still reserve stem-loop structure and high specificity for single nucleotide mismatch discrimination.

2.2.2 Substrates for Molecular Beacon Arrays

Several types of substrates are used in microarrays, such as membrane filters, glass slides and hydrogel films (29).

Glass slides have been a favored solid support for immobilization of probes because of their easy availability, low intrinsic fluorescence, high transparency, good thermal properties, excellent rigidity, and straightforward chemistries for surface modification. Due to the nonporous nature of glass, the labeled targets have direct access to immobilized probes without limitations of internal diffusion, enabling a high local concentration and rapid hybridization kinetics. The non porous surface also facilitates the rapid removal of excessive probes and fluorescence labeled targets. Even planar glass slides have many advantages in microarray applications; it is difficult for a structured biomolecule, such as an

antibody or a structured oligonucleotide probe, to assume its native configuration at the surface of a planar glass slide. Moreover, the immobilization capacity of the planar glass slide is limited which results in a relatively low sensitivity.

To eliminate the disadvantages of planar glass slides and improve the performance of the microarray technology, three-dimensional functionalized hydrophilic microporous gel film substrates were introduced. Combining the advantages of the porous structure and the planar surface, these hydrogel microporous films provide a high binding capacity and a solution-like environment in which the hybridization and other processes resemble a homogeneous liquid phase reaction rather than a heterogeneous liquid-solid interface reaction. These films are compatible with the state-of-the-art microarray spotters or dispensers and detection instruments. The disadvantages of the hydrogel film are as follows, first, it will require a relatively long washing time to remove the unreacted targets and, second, that it is more cumbersome to prepare the slides or more expensive to buy these slides.

In this section, we introduced the modification and activation of three different substrates for immobilizing molecular beacons.

2.2.2.1 Activation of Aminosilane Glass Slides

The aminosilane derived glass slides (Cat No. S3003, Dako) were cleaned with deionized distilled water and incubated in 5% glutaraldehyde in 0.1 M PBS buffer (pH = 7.4) for 2 hours. Then the slides were thoroughly washed twice with methanol, acetone and deionized distilled water, and dried.

The aldehyde group of glutaraldehyde is attacked by primary amino group of aminosilane and forms a covalent bond, which can be stabilized by a dehydration reaction and leads to Schiff base formation.

2.2.2.2 Preparation and Activation of Polyacrylamide Film (PAA film) Coated Glass Slides

The preparation of PAA film coated glass slides were introduced elsewhere (30-32) and summarized as follows. The glass slides were cleaned in a piranha solution (7:3 v/v mixture of concentrated H_2SO_4 and 30% H_2O_2) at 80 ˚C for 2 hour and washed thoroughly with deionized distilled water. Polymerization solution contained 1 M acrylamide, 0.02 M N, N-methylene-bis-acrylamide, 0.1% TEMED and 1 mg/ml ammonium persulfate. It was injected into the small chamber formed by a Bind-Silane treated glass slide and a Repel-Silane treated glass slide separated by two 20 μ m thicker Teflon spacer strips. The PAA films were activated by immersion in 25% glutaraldehyde in phosphate buffer (pH = 7.5) at 40 ˚C overnight, then thoroughly rinsed with deionized distilled water for 2 hours and dried.

The PAA gel films are produced by polymerization of acrylamide into linear chains and cross-linking the acrylamide chains with bis-acrylamide. Polymerization is initiated by adding ammonium persulfate and the reaction is accelerated by TEMED which catalyzes the formation of free radicals from ammonium persulfate.

In aqueous solutions, two aldehyde groups of glutaraldehyde can be easily cross-linked and glutaraldehyde is present largely as polymers of variable sizes. The unsaturated C═C bond can react with amide groups of PAA film. The free aldehyde groups sticking out of the side of each unit of glutaraldehyde polymer are readily combining with the primary amino group modified molecular beacons.

2.2.2.3 Preparation and Activation of Agarose Film Coated Glass Slides

Preparation and activation of agarose film coated glass slides were introduced elsewhere and summarized as follows (33): 1% agarose solution was prepared by adding 100 mg agarose to 10 ml deionized distilled water, mixing and boiling for 5 minutes. Then 2 ml of the agarose solution was poured over each of the aminosilane derived glass slides. After gelation of agarose, the slides were dried at 37 ˚C in a dryer over night. Before immobilization of the molecular beacon probes, the agarose films were activated by immersion in 20 mM $NaIO_4$ in 0.1 M PBS buffer (pH = 7.2) for 30 minutes at room temperature, then thoroughly rinsed twice with deionized distilled water and dried.

The vicinal hydroxyl groups of agarose can be oxidized by sodium periodate at a mild condition, forming aldehyde groups. The aldehyde groups can react with primary amino group via the Schiff base aldehyde-amine chemistry.

2.2.3 Fabrication of Molecular Beacon Arrays

2.2.3.1 Spotting of Molecular Beacon Arrays

All molecular beacon arrays were manufactured by the Cartesian Technologies PA Series of microarray spotting workstation, PixSys 5500. ChipMaker pin CPM3 was used to perform molecular beacon array spotting. The spotting diameter of CMP3 pin is 90 to 100 μm and the delivery volume of each spot is about 600 pL.

Spotting solutions were obtained by dissolving molecular beacon probes in sodium carbonate buffer (0.1 M, pH = 9.0) at the desired concentration.

After spotting, the agarose films and PAA films coated glass slides were incubated in a humid chamber at room temperature overnight and washed with 0.1% Tween, deionized distilled water and dried. Glutaraldehyde derived glass slides were incubated in a humid chamber at room temperature for 2 hours and at 37 ˚C for 2 hours. Then the slides were washed thoroughly in 0.1% Tween, distilled water and dried.

The Schiff base reaction is reversible at acid pH. For greater stability, the Schiff base was reduced with sodium borohydride. The sodium borohydride solution was prepared by dissolving 1.5 g NaBH4 in 450 ml phosphate buffered saline (PBS), then adding 133 ml 100% ethanol to reduce bubbling. Prepare the solution just before use and treat the molecular beacon arrays in the solution for 5 min at room temperature. This treatment also blocks unreacted free aldehyde groups by reducing them.

2.2.3.2 Immobilization Capacities of Different Substrates

To assess the immobilization capacity of different substrates, a serially diluted molecular beacon probes from 100μM to 1μM in spotting solutions were prepared and used to fabrication the molecular beacon arrays.

After immobilization and washing, the fluorescence images of the molecular beacon arrays are collected at the same laser power and PMT gain with a confocal microscope. The fluorescence intensities were extracted by ImageJ software and plotted in Figure 2.3(A).

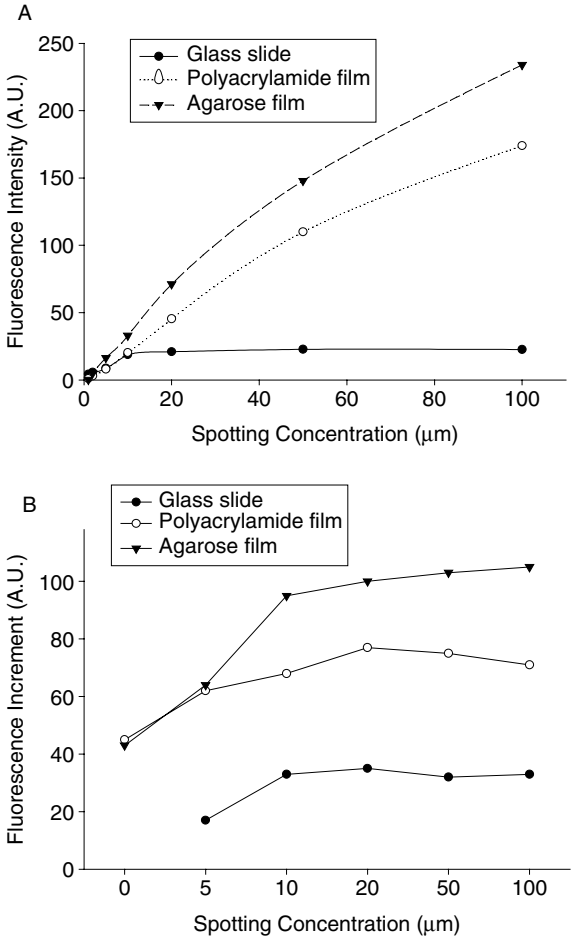

FIGURE 2.3. (A) Fluorescence intensity versus spotting concentration of molecular beacon array (B) Fluorescence intensity increment versus spotting concentration after hybridization with perfect matched targets in hybridization solution containing 10mM target in 20 mM Tris-HCl (pH = 8.0) and 10 mM $MgCl_2$.

The fluorescence intensities of molecular beacons immobilized on the glass slides increase with the increasing of spotting concentration. But the fluorescence intensities are steady when the spotting concentration is higher than 10μM, which indicate a saturated immobilization capacity of the slides. The results consist with the saturated concentration of common linear oligonucleotide probes on glass slides.

There is a nearly linear relationship between the spotting concentration and fluorescence intensity till 100μM for molecular beacons immobilized on the agarose films and the PAA films. But the agarose films show a liitle higher immobilization capacity than that of the PAA films. The tendency of the fluorescence intensity curves also indicates unsaturated immobilization capacity on both films. Further increase the spotting concentration will lead to increase of fluorescence intensities.

Further experiments were conducted to investigate the fluorescence recovery after the molecular beacon arrays hybridized with the perfectly matched targets. The results of hybridization reaction performed in hybridization solution containing 10mM target in 20 mM Tris-HCl (pH = 8.0) and 10 mM $MgCl_2$ were plotted in Figure 2.3(B). Experiments with other concentration of targets and $MgCl_2$ showed similar results.

The fluorescence intensity increments are low and showed no dependence on spotting concentration when it was higher than 10μM for molecular beacon arrays immobilized on the glass slides. It can be attributed to saturated immobilization capacity at 10μM.

The fluorescence intensity increment increase with the spotting concentration, but the increment is slow when the spotting concentration is higher than 10μM for molecular beacon arrays immobilized on the agarose films. We can see the same tendency in molecular beacon arrays immobilized on the PAA films at lower spotting concentration. But it is supervising to see the fluorescence intensity increment decrease when the spotting concentration is higher than 20μM. We contribute this decrease to the relatively lower immobilization capacity compared with the agarose films. The steric hindrance caused by the lower immobilization capacity and the higher immobilization density will retard the formation of stem structure of molecular beacons and would reduce the number of molecular beacons available for conformation change and fluorescence increment. The high density of molecular beacon probes also retards the diffusion of the target molecules.

We selection 10μM as spotting concentration based on the results and discussions above.

2.3 Hybridization of Molecular Beacon Arrays

2.3.1 Instrumentation and Software

All hybridization fluorescence images were collected by a laser scanning confocal microscope, Leica TCS SP. The 488 line of a Kr-Ar ion laser was

employed as excitation source and 10X objective was used in all experiments. The standard FITC filter setting was used in fluorescence images collection. The accumulation of 4 times (in about 4 seconds) was used in image collection to reduce the random electronic noise. In most of time serial images collection, images were collected every minute for the first 20 minutes and every 5 minutes for the following time to reduce the potential photo bleaching of the fluorescein. If not specified, images were collected at the following conditions: laser power and PMT gain settings are carefully adjusted that the average fluorescence intensity of spots in an array is about 90% of the saturated value (255) before annealing. The setting should not be changed during the collecting process.

A fluidic sample cell made of anodized aluminum was fabricated, on which a molecular beacon array was mounted. The cell can be directly mounted on the microscope stage for real time fluorescence observation during the annealing and the hybridization process. Hybridization buffers and target solutions were pumped into the fluidic cell with a peristaltic pump.

Fluorescence images were analyzed with ImageJ version 1.27. ImageJ is a public domain Java image processing program inspired by NIH Image. It can be freely downloaded from http://rsb.info.nih.gov/nih-image/index.html.

In all images of this section, the molecular beacon probes were spotted on the substrates in triplet format. From the left to the right, the probes are MB1 (noncomplementary to T2), MB2 (perfectly matched with T2), and MB3, MB4, MB5 (single central base mismatched with T2).

2.3.2 Annealing of Molecular Beacon Arrays

When the molecular beacon arrays are allowed to be dry or incubated in buffers containing no cations, quench efficiency is low and high fluorescence background image of the molecular beacon arrays can be registered. It is because the negative charged phosphate backbone of the oligonucleotide would hinder the formation of the stem structure of the molecular beacon probes. The emission from the fluorescein can't be efficiently quenched without a stable stem structure.

In order to improve the signal-background-ratio, it is important to select the ion strength, especially divalent cations to counteract the negative charge of the phosphate backbone and to stabilize the stem structure.

2.3.2.1 Annealing Process of Molecular Beacon Arrays

The fluorescence images were collected for one hour after the hybridization buffer containing different concentration of $MgCl_2$ in 20 mM Tris-HCl (pH = 8.0) were pumped into the reaction cell. The fluorescence intensities of all the molecular beacons immobilized on the different substrates were averaged and normalized by the fluorescence intensity before annealing. Two typical plots were shown in Figure 2.4.

Figure 2.4 (A) show the annealing process of the molecular beacon arrays in hybridization buffer containing 10mM $MgCl_2$. The fluorescence intensities

decrease with time for the molecular beacon arrays immobilized on all substrates. For the glass slides immobilized ones, the process is relatively faster and it complete in about 5 minutes. For the PAA and agarose film immobilized ones, the process is slower and complete in about 20 minutes.

Figure 2.4(B) show the annealing process of the molecular beacon arrays in hybridization buffer containing 500mM $MgCl_2$. Compared with the results in Figure 2.4 (A), the annealing process is much faster for the PAA film and the agarose film immobilized arrays.

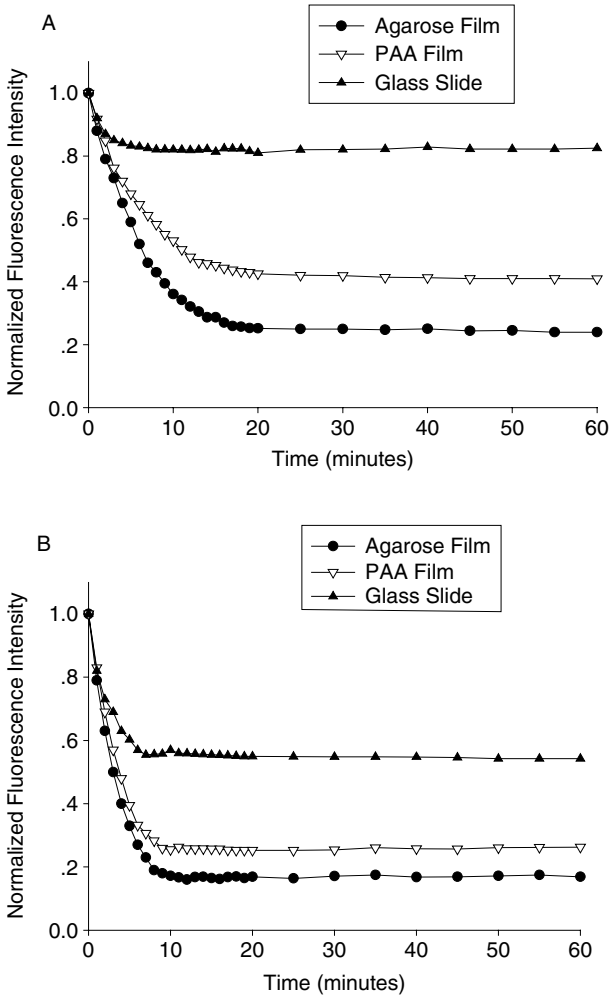

FIGURE 2.4. Normalized fluorescence intensity versus time of the molecular beacon arrays immobilized on the different substrates. The fluorescence intensity was the average of all molecular beacons on the substrates. The hybridization buffer is 20 mM Tris-HCl (pH = 8.0) and (A) 10 mM, (B) 500 mM $MgCl_2$.

The annealing time course in Figure 2.4 indicates that the annealing process complete in 20 minutes for arrays in lower concentration $MgCl_2$ buffer. So we choose 30 minutes annealing time for all the experiments in the following sections of this thesis.

2.3.2.2 Annealing Properties in Different Ion Strength

The relationship between the normalized fluorescence intensity and $MgCl_2$ concentration is illustrated in Figure 2.5. In the case of the glass slide immobilized molecular beacon arrays, the fluorescence background decrease with the increase of the $MgCl_2$ concentration. When the concentration of $MgCl_2$ reaches 100 mM, no significant changes can be observed after incubation. The fluorescence intensity of the molecular beacon arrays in hybridization buffer containing 500 mM $MgCl_2$ is about 60% of the initial intensity. In the case of the agarose film immobilized arrays; low concentration of $MgCl_2$ can effectively maintain the stem structure and quench the fluorescence. The fluorescence intensity is just about 20% of the initial intensity in hybridization buffer containing 10 mM $MgCl_2$. Further increasing of $MgCl_2$ concentration has little effect on improving the quench efficiency. The fluorescence intensity curve of PAA film immobilized arrays is similar to that of agarose film immobilized ones. This indicated similar hydrophilic microenvironments provided by the PAA films and the agarose films.

The quench efficiency is higher than 99% in bulk solutions containing 1 mM to 5 mM $MgCl_2$.

There are two effects contributed to the decrease in quenching efficiency of the agarose film and the PAA film immobilized molecular beacon arrays: first, there are still some surface effects which destabilize the stem

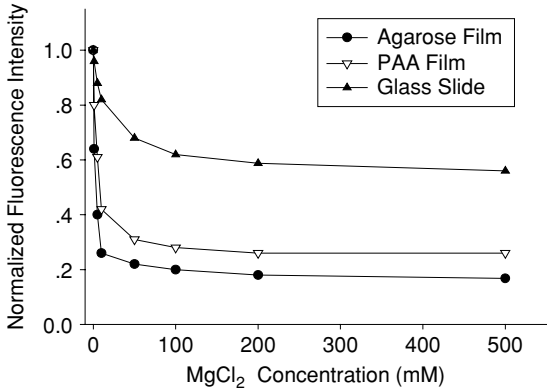

FIGURE 2.5. Normalized fluorescence intensity versus $MgCl_2$ concentration of the molecular beacon arrays immobilized on the different substrates. The fluorescence intensity is the average of all molecular beacons on the substrates. The hybridization buffer is 20 mM Tris-HCl (pH=8.0) and 500 mM $MgCl_2$.

structure of molecular beacons. Second, steric effects caused by high immobilization density retards the formation of stem structure and lower the quench efficiency.

2.3.3 Hybridization of Molecular Beacon Arrays

To investigate the specificity of the immobilized molecular beacons, hybridization solutions containing different ion strength were applied to the molecular beacon arrays on the different substrates. In all images of this section, the molecular beacon probes were spotted on the substrates in triplet format. From the left to the right, the probes are MB1 (noncomplementary to T2), MB2 (perfectly matched with T2), and MB3, MB4, MB5 (one central base mismatched with T2), respectively.

2.3.3.1 Hybridization in Different Ion Strength Solutions

Figure 2.6 displayed the hybridization results of the molecular beacon arrays immobilized on the glass slides in hybridization buffers containing 5 mM, 50 mM and 500 mM $MgCl_2$, respectively. The concentration of target T2 was 10mM. The background and hybridization fluorescence intensities were extracted with ImageJ software and the fluorescence intensity increments are calculated.

When the hybridization buffers containing 5 mM $MgCl_2$ was applied, the fluorescence intensity decreased. We attribute it to photo bleaching by continuous laser scanning. For hybridization buffer containing 50 mM $MgCl_2$ and 500 mM $MgCl_2$, the fluorescence intensity increment of the perfectly matched probes was more than that of single base mismatched probes. The noncomplementary molecular beacon probe MB1 used as negative control also showed decrease of fluorescence.

Figure 2.7 displayed the corresponding results of the molecular beacon arrays immobilized on the PAA films. The hybridization results in hybridization buffer containing 5 mM $MgCl_2$ show that the fluorescence intensity increment of the perfectly matched probes is about two folds of that of the single base mismatched probes. The perfectly matched probes and single base mismatched probes can be easily distinguished from the image. With the increment of $MgCl_2$ concentration, the ratio of fluorescence intensity increment of the perfectly matched probes to that of the single base mismatched probes also increased, even if the increase rate was low when the $MgCl_2$ concentration was higher than 50 mM.

Figure 2.8 displayed the corresponding results of the molecular beacon arrays immobilized on the agarose films. The results are similar to those of the PAA immobilized ones. But the fluorescence increments are larger than those of the PAA film immobilized ones. The results may be attributed to the relatively lower immobilization capacity of the PAA films as discussed in section 2.2.3 and the lower quench efficiency of the molecular beacon probes immobilized on PAA film as discussed in section 2.3.2.

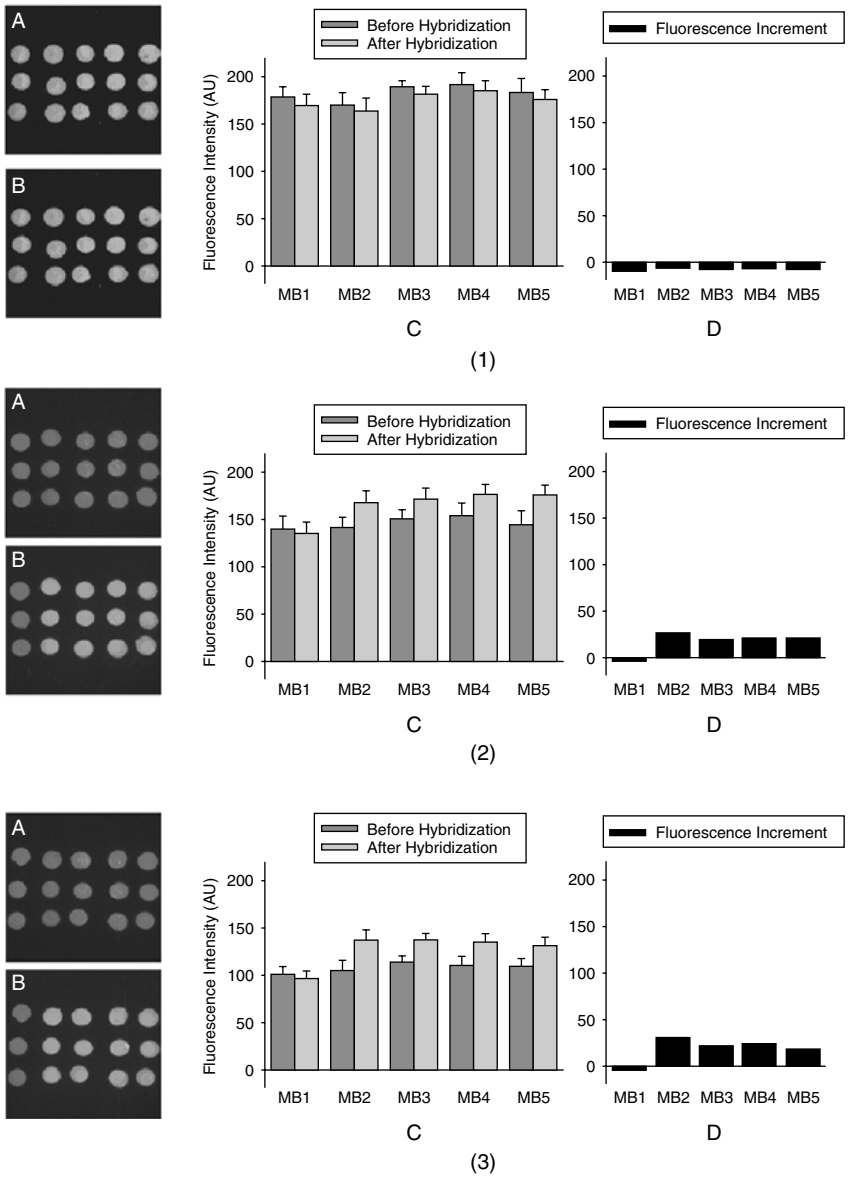

FIGURE 2.6. Images and fluorescence intensities of the molecular beacon array on a glass slide. Hybridization buffer: 10nM T2 in 20 mM Tris-HCl (pH = 8.0) containing (1) 5, (2) 50 and (3) 500 mM MgCl2. Images of (A) and (B) are fluorescence images before and after hybridization, respectively. The plots of (C) and (D) are fluorescence intensity before and after hybridization and fluorescence intensity increment, respectively.

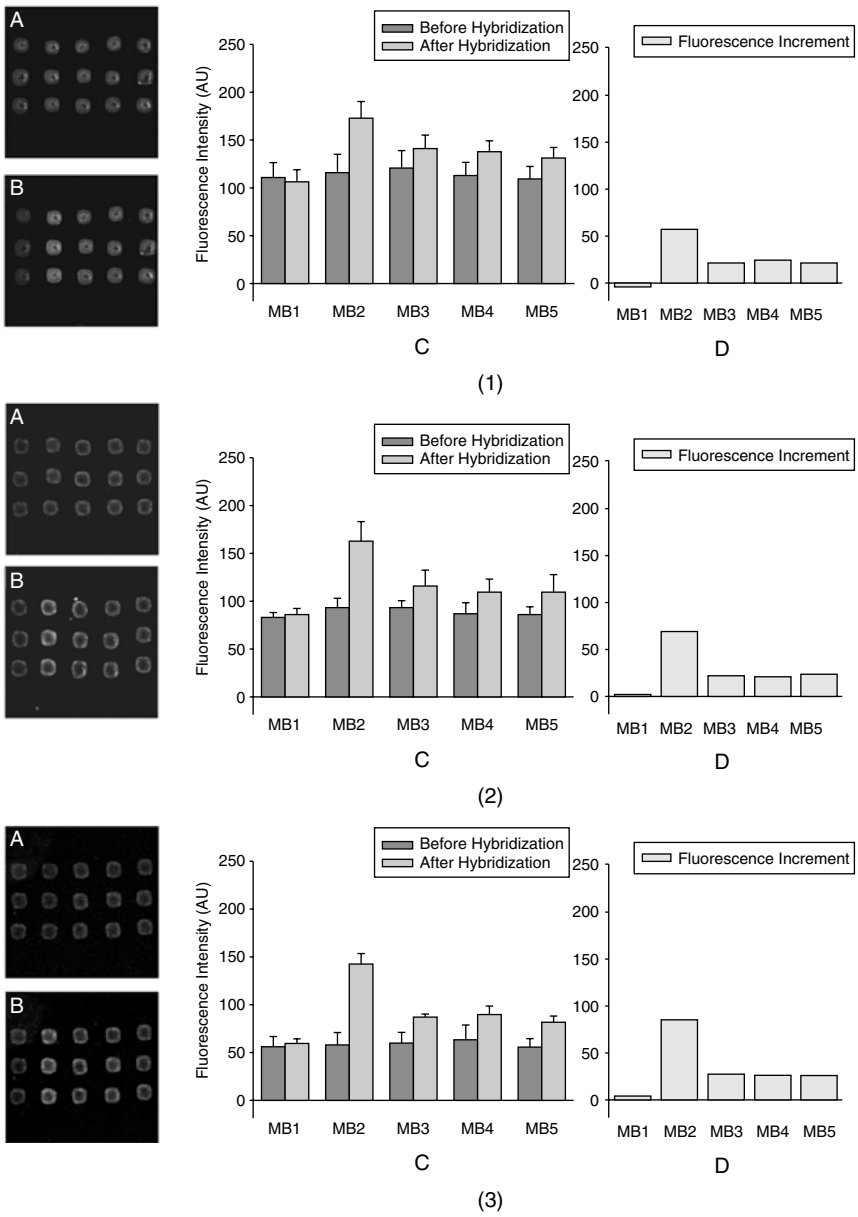

FIGURE 2.7. Images and fluorescence intensities of the molecular beacon array on a PAA film. Hybridization buffer: 10nM T2 in 20 mM Tris-HCl (pH = 8.0) containing (1) 5, (2) 50 and (3) 500 mM $MgCl_2$. Images of (A) and (B) are fluorescence images before and after hybridization, respectively. The plots of (C) and (D) are fluorescence intensity before and after hybridization and fluorescence intensity increment, respectively.

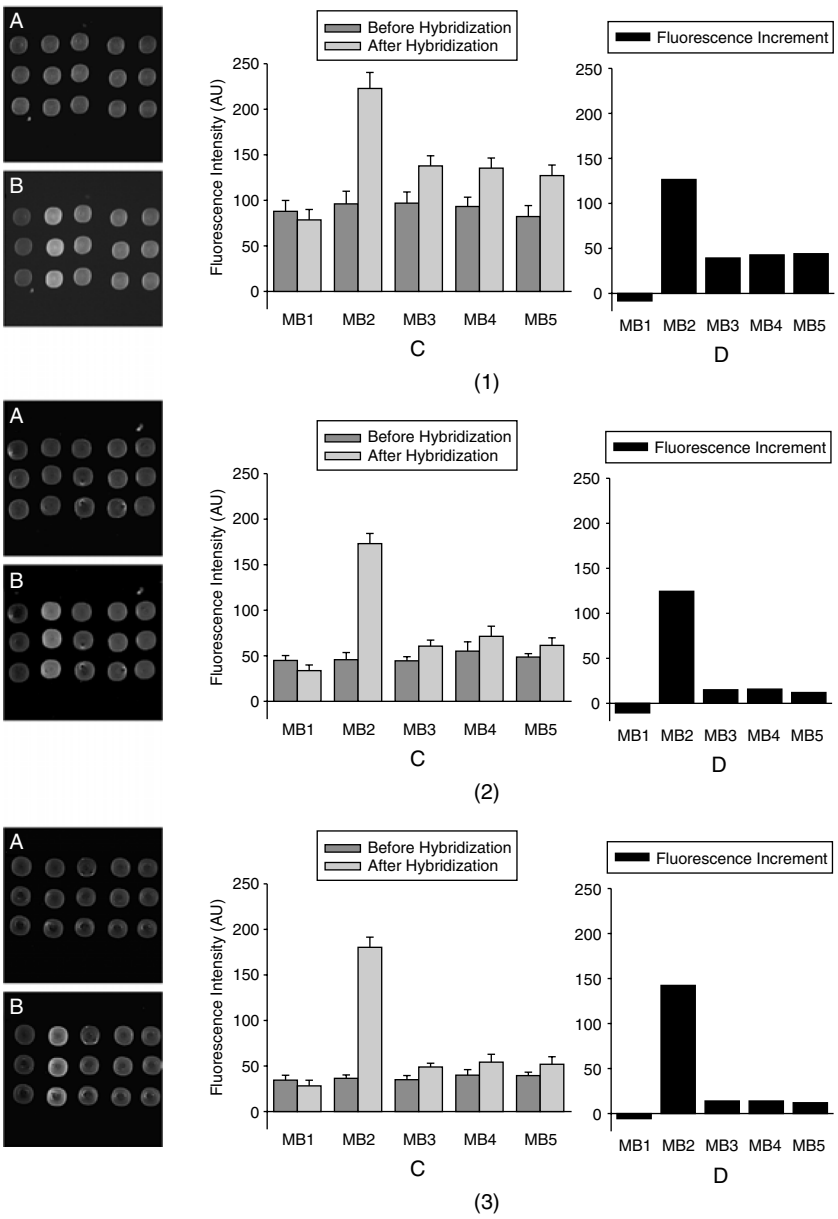

FIGURE 2.8. Images and fluorescence intensities of the molecular beacon array on an agarose film. Hybridization buffer: 10nM T2 in 20 mM Tris-HCl (pH = 8.0) containing (1) 5, (2) 50 and (3) 500 mM $MgCl_2$. Images of (A) and (B) are fluorescence images before and after hybridization, respectively. The plots of (C) and (D) are fluorescence intensity before and after hybridization and fluorescence intensity increment, respectively.

2.3.3.2 *Single Nucleotide Mismatch Discrimination Ratio in Different Ion Strength Solutions*

The single nucleotide mismatch discrimination ratio (SMR), which can be used to evaluate the ability to identify the single nucleotide mismatch, is defined as (PM-MM)/PM. PM is the average fluorescence increment of perfectly matched probes, and the MM is the average fluorescence increment of one base mismatched probes. The mismatch discrimination ratio versus $MgCl_2$ concentration was plotted in Figure 2.9.

For molecular beacon arrays immobilized on the glass slides, the SMR ratio increases from 0.09 (10 mM $MgCl_2$) to 0.3 (500 mM $MgCl_2$). The fluorescence increment is too low to get reliable ratios when the hybridization is performed in buffers containing 1mM and 5mM $MgCl_2$.

For molecular beacon arrays immobilized on the PAA films, the SMR ratio is 0.37 in 1mM $MgCl_2$, increasing to 0.63 in 10 mM $MgCl_2$ and 0.68 in 50mM $MgCl_2$. Further increasing the concentration of $MgCl_2$ will not change the SMR.

For molecular beacon arrays immobilized on the agarose films, the SMR is 0.4 in 1mM $MgCl_2$, increasing to 0.67 in 5 mM $MgCl_2$ and 0.81 in 10 mM $MgCl_2$. This ratio will increase to 0.9 in 50 mM $MgCl_2$ and there is little more increment with higher concentration of $MgCl_2$.

For solution data, the discrimination ratio is 0.98 in 1 mM $MgCl_2$ and increased to 0.99 in higher concentration of $MgCl_2$.

From this plot, we could see the SMRs of the molecular beacon arrays immobilized on the PAA films and the agarose films are similar to those in homogeneous solution. The results indicated that the molecular beacon in

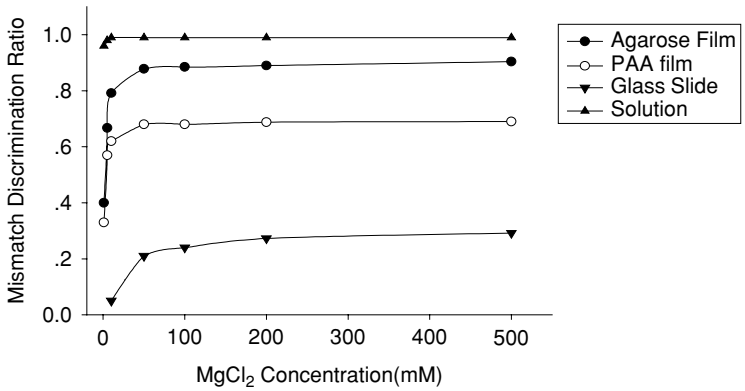

FIGURE 2.9. Mismatch discrimination ratios (SMR) of the different molecular beacons in bulk solution, immobilized on the glass slides, the PAA films and the agarose films, respectively. Discrimination ratio is defined as (PM-MM)/PM. PM is the fluorescence increment of perfectly matched probes, and the MM is the average fluorescence increment of three one-base mismatched probes. The hybridization solution is 10 nM target T2 in 20 mM Tris-HCl (pH = 8.0) with different concentration of $MgCl_2$.

solution and immobilized on the PAA films and the agarose films holds the high specificity while the glass slide immobilized one is not satisfied.

The above results can be explained by the following discussion:

Firstly, it is due to incomplete quenching of molecular beacon. From the results of annealing experiments of the molecular beacon arrays in section 2.3.2, we can find that a large part of the glass immobilized molecular beacons are not quenched. These unquenched molecular beacon probes contribute to high background and greatly reduce the number of probes available for conformation change and fluorescence restoration. High quench efficiency of the PAA films and the agarose films immobilized molecular beacons contributes to the high mismatch discrimination ratio. Moreover, the high immobilization capacity of the PAA films and the agarose films greatly improves the number of immobilized molecular beacons, which will provide more molecular beacons for conformation change and large fluorescence increment.

Secondly, the immobilization of the molecular beacon changes the electrostatic properties and the local ion strength. The environment of the glass immobilized molecular beacon probes is quite different from that they experienced in balk solution. Even high concentration hybridization buffer is used; it is difficult to counteract the interfacial effect. The PAA films and the agarose films can provide a favorable solution-like environment and hybridization in low ion strength hybridization buffer can produce reliable results. High ion strength hybridization buffers will facilitate the formation of secondary structure of PCR products and hinder the hybridization with immobilized probes in practical use.

Thirdly, considering the SMR is about 0.3 to 0.7 for immobilized linear probes employed in most of the microarray technology (31), the SMR of the molecular beacon arrays immobilized in the hydrogel microporous films are satisfying. The thermodynamic balance between the hairpin structure and the duplex formed by molecular beacon with target ensures the high specificity of the molecular beacon in target recognition and discrimination.

2.4 Hybridization Kinetics of Molecular Beacon Arrays

The real-time hybridization process at room temperature was investigated. Hybridization solutions of different ion strength buffers, target concentrations were applied to the molecular beacon arrays immobilized on the different substrates.

2.4.1 Hybridization Kinetics in Different Ion Strength Buffers

Time serial images after applying 10 nM target T2 in 10 mM $MgCl_2$ hybridization buffers to the molecular beacon arrays immobilized on the glass slides, the PAA films and the agarose films were collected. The fluorescence intensity increment were calculated by subtracting the fluorescence background (fluorescence intensity before hybridization) from the fluorescence intensity at different time and plotted in Figure 2.10 (A), (C) and (E),

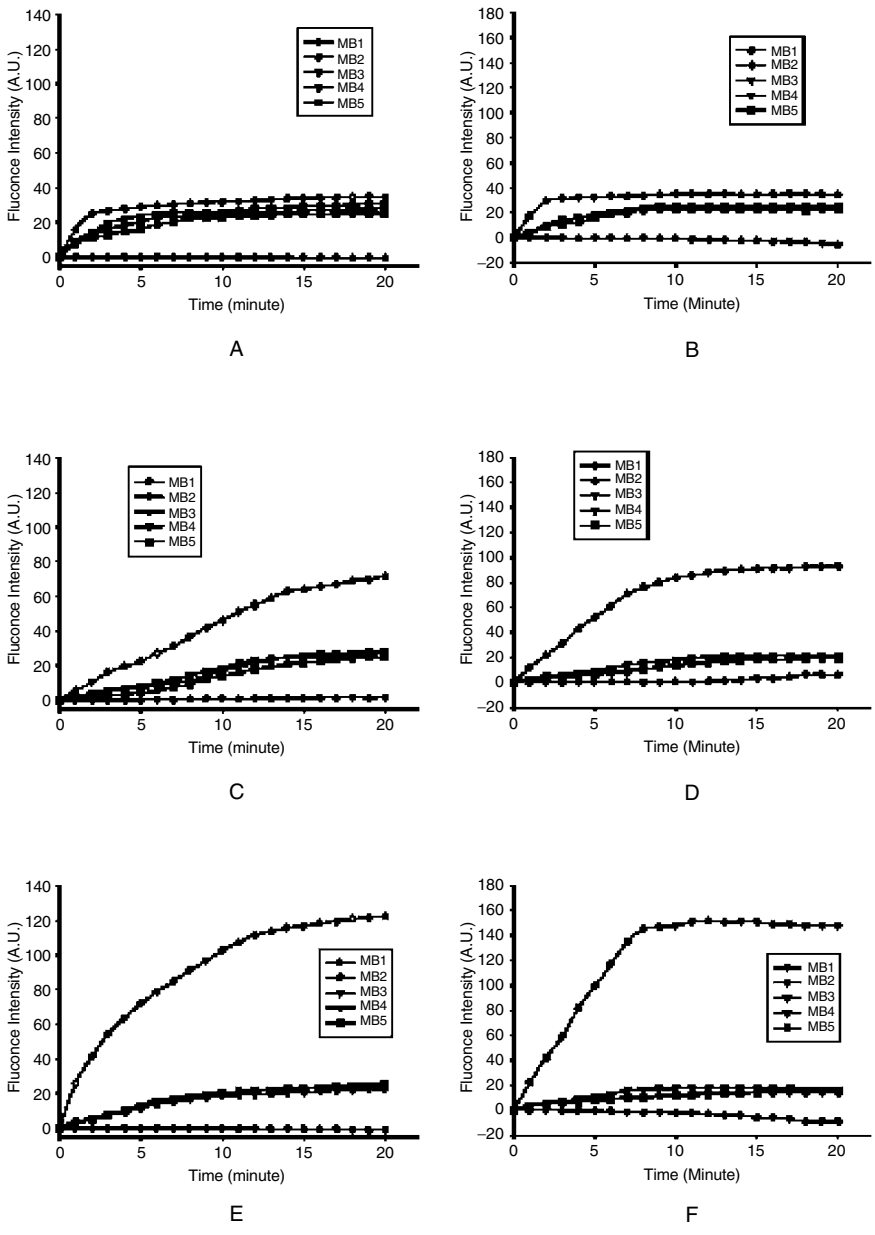

FIGURE 2.10. Fluorescence increment versus time after applying 10 nM target T2 in hybridization buffers containing 10 mM (left panel) and 500 mM (left panel) $MgCl_2$ to the molecular beacon arrays immobilized on the glass slides (A,B), the PAA films (C,D) and the agarose films (E,F).

respectively. These figures indicate that the hybridization process of the molecular beacon arrays immobilized on glass slides is so fast that 90% of the reaction completed in 4 minutes, while the reactions are much slower for the PAA films and the agarose films immobilized ones and the reaction completed in 18 minutes and 14 minutes, respectively.

The corresponding fluorescence increment versus time after applying 10 nM target T2 in hybridization buffers containing 500mM $MgCl_2$ to the molecular beacon arrays immobilized on the glass slides, the PAA films and the agarose films were shown in Figure 2.10 (B), (D) and (F), respectively. The results indicate the hybridization reactions completed in a shorter time and the fluorescence increment is larger with the increase of $MgCl_2$ concentration.

We define the hybridization time as the time needed for the fluorescence intensity increment of perfect marched molecular beacon probe reaches 90% of saturated value. The relationship between the hybridization time and $MgCl_2$ concentration was illustrated in Figure 2.11.

The results in Figure 2.11 indicate that the hybridization reaction time decreases with the increase of the $MgCl_2$ concentration. The hybridization time decreased from 25 minutes, 25 minutes and 13 minutes at 5 mM $MgCl_2$ to 3 minutes, 9 minutes and 7 minutes at 500 mM $MgCl_2$ for the glass slide, the PAA films and the agarose films immobilized arrays, respectively. The effect of $MgCl_2$ is apparent when the concentration is lower than 50mM.

The results will be discussed as follows. Firstly, the hybridization reaction time of the glass slide immobilized arrays is much shorter than that of the PAA films and the agarose films immobilized ones. It is because the

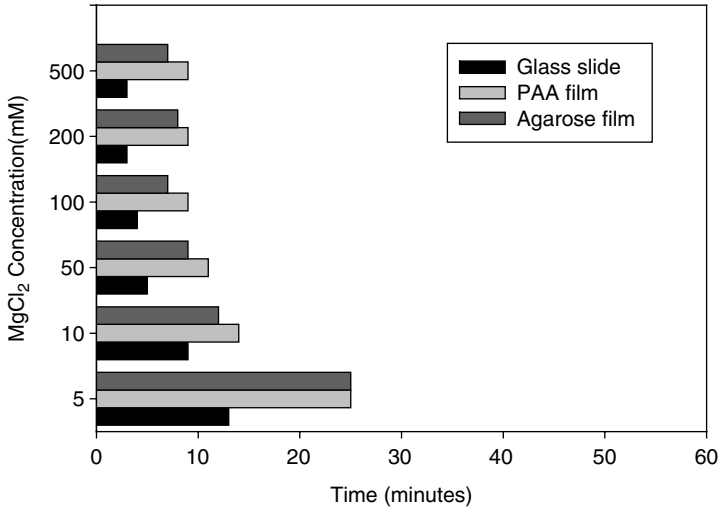

FIGURE 2.11. Hybridization time of the molecular beacon arrays immobilized on the different substrates. The hybridization solution containing 10 nM target T2 in 20 mM Tris-HCl (pH = 8.0) and different concentration of $MgCl_2$.

hybridization process in the hydrogel microporous films is mass transport limited reaction and the mass transport process is slower than the hybridization process. One of the main advantages of the glass slides based microarray technology over the traditional filter hybridization is the high diffusion rate and the short reaction time. Secondly, the hybridization reaction time decreases with the increase of the ion strength. Since the increase of the ion strength will facilitate the duplex formation and stabilization and the depletion of the target at the surface, the diffusion of target to the surface will be accelerated and the hybridization reaction will complete in a shorter time.

2.4.2 Hybridization Kinetics in Different Target Concentration Solutions

The above results indicated the agarose film immobilized molecular beacon arrays performed well in signal intensity and single nucleotide mismatch discrimination ratio.

To investigate the relationship between the fluorescence intensity and target concentration, different concentration targets in hybridization buffer containing 20 mM Tris-HCl (pH = 8.0) and 10 mM $MgCl_2$ were applied to the agarose film immobilized molecular beacon arrays.

The fluorescence intensity increment of the perfect matched probes versus time is shown in Figure 2.12. The hybridization reactions are faster when higher concentration targets are applied.

2.5 Application of Molecular Beacon Arrays

A polymorphism in codon 158 of the human ApoE gene (34), which plays a key role in the transport and metabolism of plasma cholesterol and triglyc-

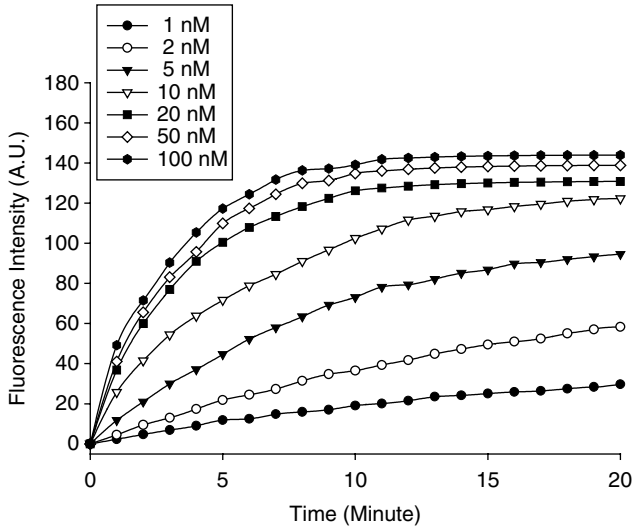

FIGURE 2.12. Fluorescence intensity increment versus time of the molecular beacon array immobilized on the agarose films after adding the hybridization solution containing different concentration target T2 in 20 mM Tris-HCl (pH = 8.0) and 10 mM $MgCl_2$.

erides, was employed to investigate the performance of molecular beacon arrays in complex environment.

2.5.1 Human Genome DNA Extraction and PCR Amplification

Human genomic DNA was extracted from whole blood cells by phenol-chloroform method.

A 218-bp DNA fragment containing the single nucleotide polymorphism of codon 158 of human apoE gene was amplified with the primer sequences: 5′-TCCAAGGAGCTGCAGGCGGCGCA (Forward) and 5′-GCCCCG-GCCTGGTACACTGCCA (Reverse) as previously described (34).

The symmetric PCR reactions were performed in a total volume of 25 μL containing 75 mM Tris-HCl (pH = 9.0), 20 mM ammonium sulfate, 0.1 mL/L Tween, 1.5 mM $MgCl_2$, 500 nM of each primer, 200 μM dNTPs, 100 mL/L DMSO, and 1 unit of Taq polymerase. Amplification condition consisted of an initial 10-min denaturation at 94 ˚C followed by 40 cycles of 30 s of denaturing at 94 ˚C, 30 s of annealing at 65 ˚C, and 30 s of extension at 70 ˚C.

The asymmetric PCR mixture contained all the reaction components in identical amount as that in symmetric PCR except that forward primer concentration was 50nM. Amplification condition was the same as the symmetric PCR.

Fragmented PCR products were prepared as symmetric PCR reactions described above with the exception of using 160 μM dTTP and 40 μM dUTP instead of 200 μM dTTP. Amplification condition was the same as symmetric PCR except that the annealing temperature was 55˚C. The PCR products were fragmented by adding 2U of UNG and incubating at 37˚C for 60 minutes, followed by heating the solution to 95˚C for 5 minutes to inactivate the enzyme.

Aliquots of 2 μL PCR products were electrophoresed on 2% agarose gel and visualized by ethidium bromide staining. The Electrophoretic image is shown in Figure 2.13 (A). Lane 1 and lane 2 are 218-bp symmetric and asymmetric PCR products, respectively. Lane 3 and lane 4 are symmetric PCR products amplified from the PCR mixture containing dUTP before and after fragmentation with UDG, respectively. In lane 4 the fragmented PCR product appears as a smear.

2.5.2 Genotyping by PCR-RFLP

The apoE genotype was indentified by a polymerase chain reaction restriction fragment length polymorphism (PCR-RFLP) method. PCR-RFLP was carried out by adding 2 units of BstH2 I ((prototype *Hae* II, Sibenzyme Ltd.,Russia) to 20 μL symmetric PCR products for 2 h at 65 ˚C and analyzed by 4% agarose gel. The Restriction site of BstH2 I is RGCGC∧Y (R: purine, adenine and/or guanine; Y: pyrimidine, thymine and/or cytosine).

The Electrophoresis image of the PCR products was shown in Figure 2.13 (B). Lane 1 and lane 2 depict the 218-bp PCR product before and after BstH2 I digestion, respectively. Lane 2 depicts a C/T heterozygote.

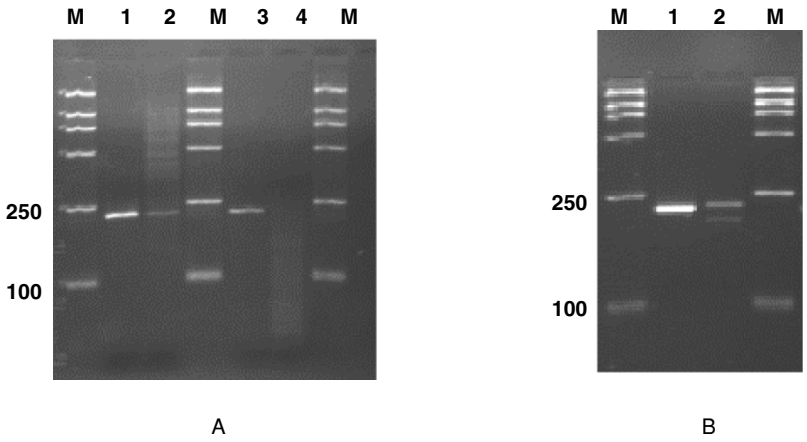

FIGURE 2.13. (A) Electrophoretic image: Lane 1 and lane 2 are symmetric and asymmetric PCR products, respectively. Lane 3 and lane 4 are PCR products before and after fragmentation with uracil-N-glycosylase, respectively. (B) Electrophoretic image: Lane 1 and lane 2 depict the 218-bp PCR product before and after HaeII digestion, respectively. Mutation from C to T causes the loss of restriction site. Lane 2 depicts a C/T heterozygote.

2.5.3 Hybridization of PCR Product to Molecular Beacon Arrays

20μL asymmetric and fragmented PCR products were added to 80μL hybridization buffers (20 mM Tris-HCl (pH = 8.0) and 10 mM $MgCl_2$) and pumped to hybridization cell for 30 minutes.

The hybridization images of asymmetric and fragmented PCR products were displayed in Figure 2.14 (A) and (B), respectively. The fluorescence intensity increments are shown in Figure 2.14 (C) and the discrimination ratio were calculated to be 0.61 and 0.64. Though the discrimination ratio is lower than that of the oligonucleotide targets at the same concentration of $MgCl_2$, it is good enough for practical applications.

2.6 Conclusions

We investigated and compared the immobilization, annealing, hybridization and application of molecular beacon arrays on different substrates, and demonstrated the excellent performance of hydrogel films as the immobilization substrate for molecular beacon microarray.

Molecular beacon array has shown many advantages over conventional microarray. Firstly, no target labeling is needed. Labeling is an important step in most of the microarray-based target preparing protocols. It is not only time consuming, and rather expensive, but also can change the levels of targets originally present in the sample. The use of molecular beacon allows one to eliminate target labeling. Secondly, no washing step is required. Since the

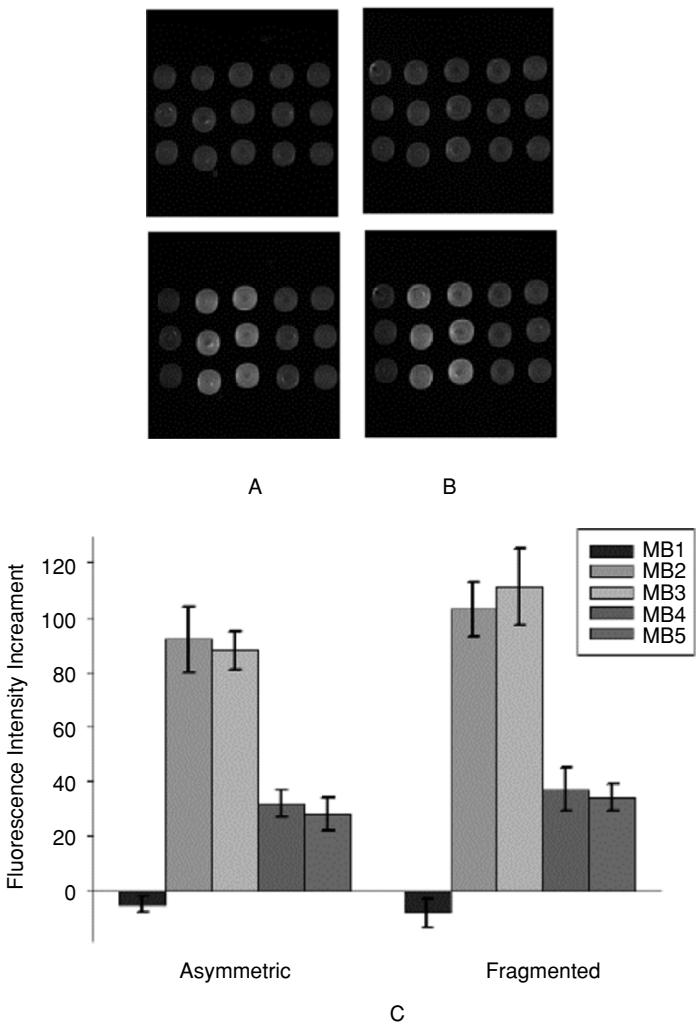

FIGURE 2.14. Fluorescence images before (up) and after (down) hybridization with asymmetric (A) and fragmented (B) PCR products, respectively. C) The fluorescence intensity increments after hybridization with asymmetric and fragmented PCR products.

unlabeled targets will not contribute to the fluorescence background and specificity of the molecular beacon probes are guaranteed by thermodynamic property of hairpin structure, washing step is not necessary. The high background caused by washing problem in conventional porous film microarray is resolved. It will also simplify the miniature device, such as lab-on-chip, design without considering washing problems in small volume. Moreover, the hybridization process can be easily monitored in real time and more reliable

results can be obtained from the hybridization dynamic curves. Thirdly, high specificity of molecular beacon ensures the single oligonucleotide mismatch can be easily detected. The presence of hairpin structure maximizes the specificity of molecular beacon probes. Furthermore, unlike linear probes, molecular beacon probes are insensitive to mismatch type and position, which greatly simplify probe design.

We investigated the annealing and hybridization process of molecular beacon array on different substrates in different hybridization buffers. For glass slide, the interfacial effects destabilize the hairpin structure of molecular beacon and lead to high background. Hydrogel films, combining the fast reaction speed of glass slide and solution-like environment provides an ideal support for molecular beacon arrays. Low fluorescence background after annealing and high mismatch discrimination ratio promise great capacities for practical applications of hydrogel film immobilized molecular beacon array. Further experiment with PNA molecular beacons may take the advantages of uncharged backbone of PNA and further improve the single nucleotide mismatch discrimination ratio.

The instrumentation for fabricating molecular beacon microarrays and signal detection are compatible with the state of art microarray technique. Other high density microarray fabrication technique, such as light-directed synthesis, liquid dispersing method and molecular stamping, allows fabricate the high density molecular beacon microarray economically.

It is expected that molecular beacon microarrays can perform high-throughput mutation analysis and disease diagnosis in a parallel, cost saving and label-free way.

3. Microarray Based Melting Curve Analysis Method for Single Nucleotide Mismatch Detection

3.1 Melting Curve Analysis Methods

DNA fragments can be distinguished from each other by their melting properties. The melting properties of a short piece of DNA, such as a PCR product, are very strongly influenced by the size, sequence composition, and mismatch bases. Various melting curve based analysis methods were developed in the last few years (12). In these methods, melting can be performed by an increasing gradient of some denaturing agent, such as temperature, electronic field, ion strength, etc. In this section, several melting curve analysis methods were briefly reviewed.

3.1.1 Homogeneous Melting Curve Analysis Methods

A number of melting curve analysis methods has been developed that allow fully homogeneous assays to be performed.

Melting curve analysis of single nucleotide polymorphism (McSNP) is a method combining a classic approach, restriction enzyme digestion, with a melting curve analysis method (35). After PCR, products are digested with the appropriate restriction enzyme for the SNP of interest. This creates different length and melting temperature fragments between the two SNP alleles. Then melting curve measured by slowly heating DNA fragments in the presence of the dsDNA-specific fluorescent dye SYBR Green I. As the sample is heated, fluorescence rapidly decreases when the melting temperature of a particular fragment is reached. By analyzing the melting curve, the genotype of the sample can be determined.

Another approach of melting curve analysis method is based on fluorescence resonance energy transfer (FRET) (36). It involves two adjacent, fluorescently labeled probes, one overlapping the SNP position and acting as a donor while the other acting as an acceptor (quencher). The quench efficiency is strongly dependent on the distance of the donor and the acceptor. The single nucleotide mismatch at the SNP position will significantly reduce the melting temperature and the genotype can be determined.

Though many efforts have been devoted to the automatization of melting curve analysis in homogeneous solution, it is difficult to meet the high-throughput requirement in post-genome era.

3.1.2 Heterogeneous Melting Curve Analysis Methods

Dynamic allele specific hybridization (DASH) is a fast, cheap, robust and accurate genotyping method, which is suitable for medium scale genetic association studies (37). DASH involves a PCR with a biotinylated forward primer, immobilizing the resulting PCR products to a 96-well streptavidin-coated plate, denaturing away the reverse strand and probing the region of interest. After that, the dsDNA-specific fluorescent dye SYBR Green and the probe are added. Then the probe is gradually melted away, and since a mismatching probe melts at a lower temperature compared with the matched probe, the samples can be genotyped. DASH is a low cost and flexible method for SNP detection. However, like dot-blot, only one to two assays can be performed with each sample.

Microarray based melting curve analysis method was firstly reported by Mirzabekov et al. (38-39). The PAA gel pad immobilized oligonucleotide probes were used to identification of β-thalassemia mutations. With the melting curve analysis methods, the base changes and the homozygous and heterozygous β-thalassemia mutations can be reliably identified. Mirzabekov et al also investigated the thermodynamic properties for perfect and mismatched short oligonucleotide (8 bp) in the gel pad with equilibrium melting curves and compared the results with the solution data.

Another approach is to use electronic field instead of the temperature to denature the duplex. The NanoChip® Workstation provided by Nanogen Inc. can perform this kind of electronic stringency hybridization of the target DNA to the array, a precisely controlled negative electric field is used to

dehybridization of the target from the mismatched capture probes and facilitate the discrimination of the matched and mismatched probes (40).

The disadvantage of the gel pad based system is the complex fabrication procedure and the high cost of the gel pad substrate. The Nanochip system also needs a high coat workstation and biochips.

3.2 Melting Curves of Duplexes in Solution and on Microarrays

3.2.1 Microarray Experiment Setups

Melting experiments on microarray were performed in real time on an experimental setup illustrated in Figure 2.15. The setup consists of detection optics, a hybridization chamber, a water bath temperature controlling system and an XY stage.

In our system, Leica confocal microscope TCS SP is used as detecting system. Compared with non-confocal system, low focus depth of confocal optics can effectively reject unwanted fluorescence from the solution and improve the signal-background ratio. The fluorescence images were collected in a scanning mode and the time for image collection was about 4 second (4 accumulation each image). The fluorescence change during the image collection can be ignored.

The hybridization chamber is composed of a 100 μL hybridization cell, an XY stage and a peristaltic pump and a valve to control the hybridization solution and buffer flowing through the pipe. The microarray can be pressed against the hybridization cell during the experiment.

Around the hybridization cell, the stage is hollowed to form a water jacket which connects a water bath reservoir.

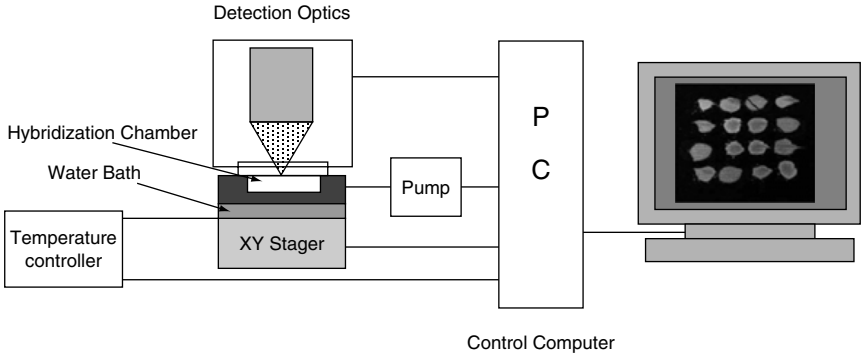

FIGURE 2.15. Experiment setup for melting curve experiments on microarrays.

3.2.2 Softwares

Fluorescence images were analyzed by ImageJ version 1.27. ImageJ is a public domain Java image processing program inspired by NIH Image. It can be freely downloaded from http://rsb.info.nih.gov/nih-image/index.html.

The nonequilibrium melting curve can be obtained by plotting the fluorescence intensities extracted by ImageJ versus temperature. The dissociation temperature (T_d) of the matched and mismatched duplexes can be determined from the nonequilibrium melting curve. We use recently issued web-based software to calculate the dissociation temperature. The software is available at http://stahl.ce.washington.edu. The software is explained in a detailed in an article published in (41).

3.2.3 The Probe and Target Sequences

The 20mer probe and 20mer, 17mer and 14mer unlabeled and fluorescein labeled probes and targets used in this section were listed in Table 2.2.

3.2.4 Melting Curves of Duplexes in Solution

Melting experiments in solution were performed by measuring absorption hypochromism on a Shimadzu 2100 UV-VIS spectrophotometer equipped with a circulated water bath. Melting curves were measured when the temperature of the solution increased from 26 ˚C to 90 ˚C at the rate of 0.5 ˚C/min. Annealing curves were measured when the temperature of the solution decreased from 90 ˚C to 26 ˚C at the rate of 0.5 ˚C/min. Absorbance date at 260nm were collected at 1 ˚C intervals.

The perfect matched and single central base mismatched probes and targets were diluted to the final concentration of 1μM each strand in a melting buffer containing 10mM PBS (pH=7.0) and 1M sodium chloride.

TABLE 2.2. The probe and target sequences

Symbol	Sequence
P20G	5′-NH_2-AG GAG GCT A**G**T TCT CTC AGG
P20C	5′-NH_2-AG GAG GCT A**C**T TCT CTC AGG
P20A	5′-NH_2-AG GAG GCT A**A**T TCT CTC AGG
P20T	5′-NH_2-AG GAG GCT A**T**T TCT CTC AGG
T20C	3′-TC CTC CGA T**C**A AGA GAG TCC
T17C	3′-CTC CGA T**C**A AGA GAG TC
T14C	3′-TC CGA T**C**A AGA GAG
F20C	3′-FAM-TC CTC CGA T**C**A AGA GAG TCC
F20A	3′-FAM-TC CTC CGA T**A**A AGA GAG TCC
F17C	3′-FAM-CTC CGA T**C**A AGA GAG TC
F14C	3′-FAM-TC CGA T**C**A AGA GAG

Bold underline indicates the single nucleotide mismatch position.

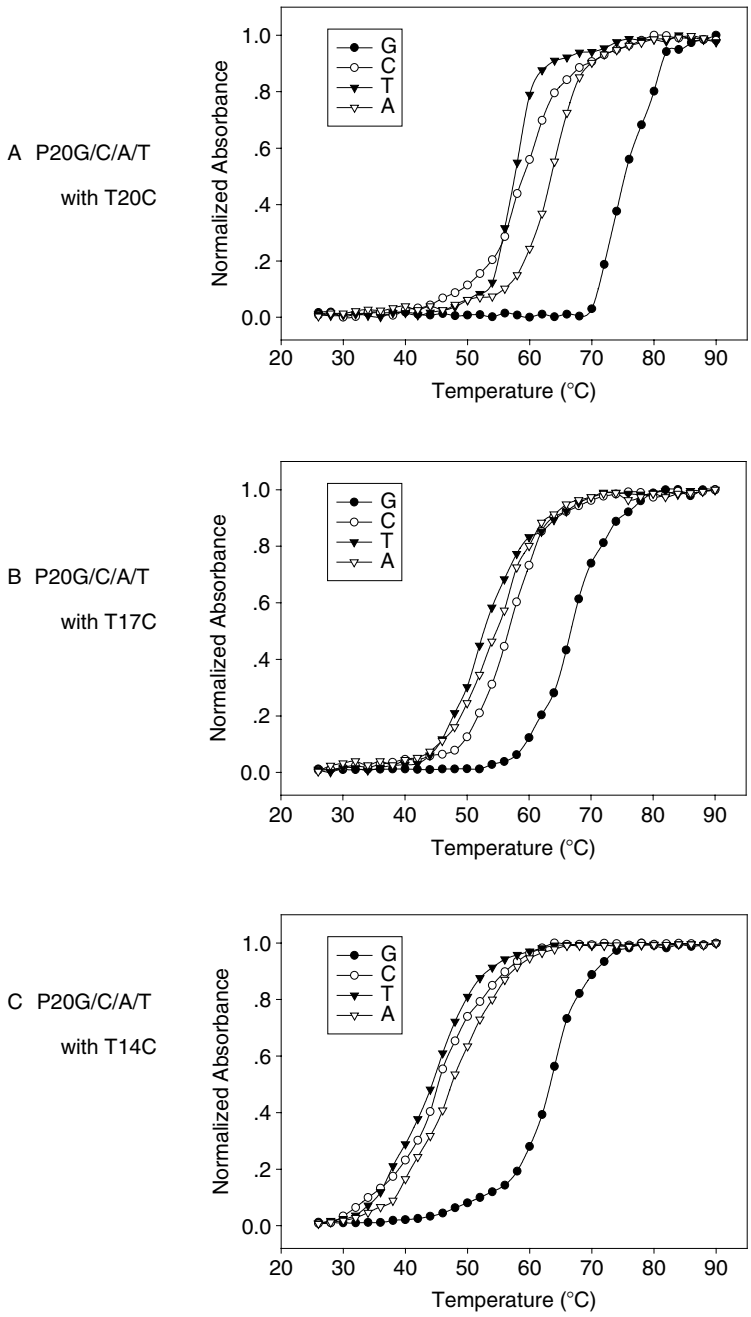

FIGURE 2.16. Normalized melting curves of perfect matched and one central base mismatched 20mer probe / 20mer target, 20mer probe /17mer target and 20mer probe/ 14mer target in solution.

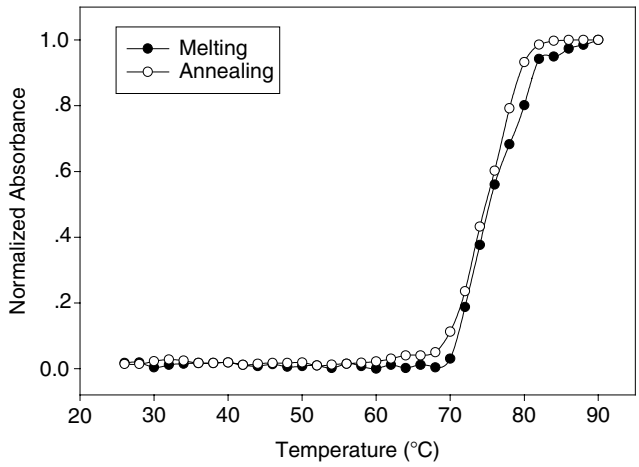

FIGURE 2.17. Normalized melting and annealing curves of the 20mer perfectly matched probe/target (P20G/T20C) in solution.

To compare the melting curves of different duplexes, we normalized the absorbance data by

$$f = (A_{260}(T_{min}) - A_{260}(T))/ (A_{260}(T_{min}) - A_{260}(T_{max}))$$

and plotted f versus temperature in Figure 2.16.

The normalized melting and annealing curves of the 20mer perfectly matched duplex, P20G and T20C, in solution were shown in Figure 2.17. The absence of hysteresis suggests that these curves were measured under equilibrium conditions and the melting process in the experiment was slow enough to reach the equilibrium at each temperature.The melting temperature, defined as the middle point of the melting transition, of different duplexes in solution was calculated and listed in Table 2.3.

The average melting temperatures of 20mer, 17mer and 14mer single central base mismatched duplexes are 60 ˚C, 54 ˚C and 45 ˚C respectively. The melting temperature differences of the 20mer, 17mer and 14mer perfect matched duplexes and one central base mismatched duplexes are 14 ˚C, 13 ˚C and 18 ˚C, respectively.

3.2.5 Melting Curves of Duplexes on Microarrays

The microarrays used for melting curve investigation were prepared as follows. The aminosilane derived glass slides (Cat. No S3003, Dako) were

TABLE 2.3. Melting temperature of different duplexes

	G/C	C/C	T/C	A/C
P20/T20	74	59	58	63
P20/T17	67	56	53	55
P20/T14	63	45	44	48

cleaned with deionized distilled water and incubated in 5% glutaraldehyde in 0.1 M PBS buffer (pH = 7.4) for 2 hours. Then the slides were thoroughly washed twice with methanol, acetone and deionized distilled water, and dried. Spotting solutions were obtained by dissolving oligonucleotide probes in sodium carbonate buffer (0.1 M, pH = 9.0) at the concentration of 100 μM. Pin-based spotting robot PixSys5500 with CMP3 pin was used to perform microarray spotting. After spotting, the glutaraldehyde derived glass slides were incubated at room temperature for 2 hours and at 37 ˚C for 2 hours and thoroughly washed in 0.1% Tween.

Melting experiments on microarrays were performed with the instrument introduced in section 3.2.1. The hybridization solutions were prepared by dissolving the targets F20C, F17C and F14C in a hybridization buffer (10mM PBS (pH = 7.0) and 1M sodium chloride) to the final concentration of 400nM. Before the melting experiments, the hybridization solutions were pumped into the hybridization cell for 30 minutes.

Fluorescence images during the melting process were collected when the temperature in the hybridization cell increased from 25 ˚C to 70 ˚C at the rate of 0.5 ˚C/min. Fluorescence images during the annealing process were collected when the temperature in the hybridization cell decreased from 70 ˚C to 25 ˚C at the rate of 0.5 ˚C/min. The fluorescence images were collected every 2 ˚C and they were accumulation of four scanning to reduce the electronic noise. The fluorescence intensity versus temperature is plotted in Figure 2.18.

The melting and annealing curves of the 20mer perfectly matched duplex P20G/F20C, and one base mismatched duplex P20T/F20C on microarray were shown in Figure 2.19. Compared with results in solution shown in Figure 17, the apparent hysteresis in annealing curves suggests that the melting curves were not measured at the equilibrium state. It can be seen from the Figure 2.19 that the mismatched targets anneal at a slower rate than the matched on do.

The dissociation temperature T_d, distinguished from the melting temperature determined from the equilibrium melting curves, is defined as the temperature at which half of the duplex were dehybridized. With the web based software provided by Washington University, microarray melting data can be normalized and the dissociation temperature can be calculated. The results provided by the software were listed in Table 2.4.

The average melting temperatures of 20mer, 17mer and 14mer one central base mismatched duplexes are 40.4 ˚C, 34.2 ˚C and 32.4 ˚C respectively. The melting temperature differences of the 20mer, 17mer and 14mer perfect matched duplexes and one central base mismatched duplexes are 4.4 ˚C, 5.2 ˚C and 5.8 ˚C, respectively.

3.2.6 Discussion

The results in solution and on microarrays will be compared and explained by the following discussion.

Firstly, comparing Figure 2.16 and Figure 2.18, the melting curves of the duplexes on microarrays are broadened and depressed relative to the

A P20G/C/A/T with F20C

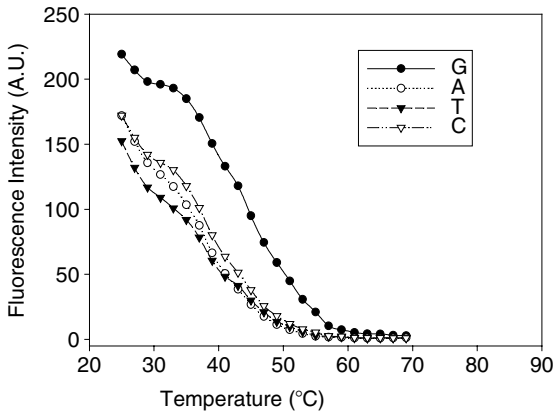

B P20G/C/A/T with F17C

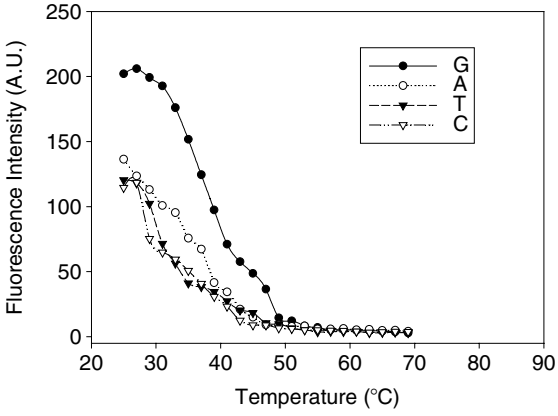

C P20G/C/A/T with F14C

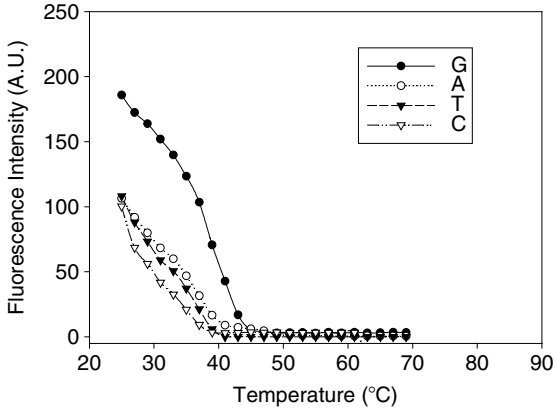

FIGURE 2.18. Melting curves of perfect matched and one central bas mismatched 20mer/20mer, 20mer/17mer and 20mer/14mer probe/target on microarrays.

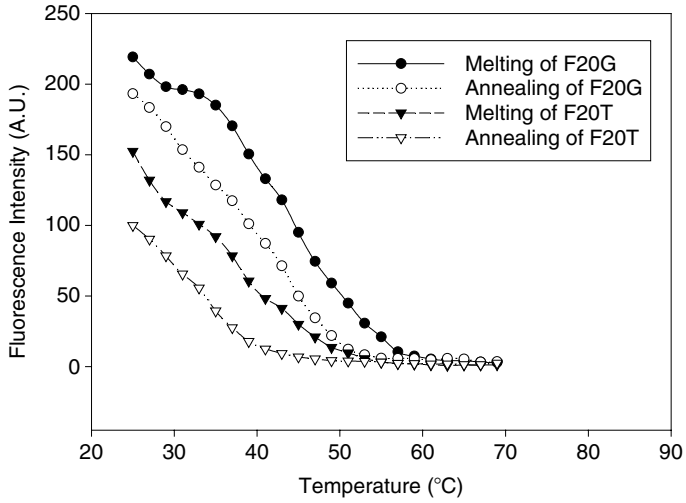

FIGURE 2.19. Melting and annealing curves of the 20mer perfectly matched probe/target (P20G/T20C) and one base mismatched probe/target (P20G/T20T) on a microarray.

corresponding duplexes in solution. The melting properties are greatly affected by the local dielectric environment and ion strength. The low local ionic strength at the liquid-solid interface, which is induced by the low dielectric constant siloxane layer and the high negative charged phosphate backbones, alters the melting behavior of duplexes on the microarrays.

Secondly, compared with the solution data, the melting curves on microarrays move to lower temperature, which indicates the lower thermal stability of duplexes on microarrays. It can also be attributed to the low ion strength and the high negative charges at the interface.

Thirdly, the duplexes in solution reach equilibrium state at each temperature, while the duplexes on microarrays do not reach at the same heating rate. The results indicate it may take several hours to get equilibrium curves on microarray, which makes the diagnostic applications of equilibrium curves analysis impractical. In next section, we will report the non-equilibrium melting curves analysis, which can give reliable results in about one hour.

Finally, the melting temperature difference between the perfect matched duplexes and single central base mismatched duplexes is decreased with increase of duplex length. In solution, the difference is more than 10 ˚C.

TABLE 2.4. Dissociation temperature of different duplexes

	G/C	C/C	T/C	A/C
P20/F20	45.0	38.8	41.7	40.8
P20/F17	39.4	34.0	32.8	35.9
P20/F14	38.2	29.8	32.7	34.6

Considering the sharpness of melting curves, it is easy to distinguish the matched duplexes from the single central base mismatched duplexes. In contrast, on microarrays, the dissociation temperature difference is about 5 °C. The broadened melting curves make it more difficult to distinguish the matched duplexes from the mismatched ones. In state-of-the-art microarray technology, hundreds to thousands of oligonucleotide probes are immobilized on the glass slides. It is really difficult to normalized thermodynamic properties and hybridization conditions of these probes. Melting curves analysis may provide a solution to the contradiction of high throughput and high reliability.

3.3 Application in Detecting HBV Mutations

Hepatitis B is a global health problem with a considerable morbidity and mortality. Some mutations of HBV appear to be closely related with hepatocellular carcinoma (HCC), one of the most common human cancers (42-43).

In this section, we constructed a microarray containing probes targeting five sets of these mutations. The GC contents and the melting temperature of the probes are over a wide range. The results demonstrate the excellent single nucleotide mismatch discrimination ability of nonequilibrium melting curve analysis method.

3.3.1 The Design of Oligonucleotide Probes

We chose five sets of probes targeting hepatitis B virus mutations related to hepatocellular carcinoma (HCC) at nt positions of 531(T to G), 546(C to T) and 587(G to A) in SHBsAg protein and 1762 (A to T) and 1764 (G to A) in core promoter region.

The 17 base oligonucleotide probes were modified with amino group at 5′ end for immobilization. The mutation position is at the center position to maximize the mismatch discrimination. The GC contents of probes ranged from 29.4% (5 GC in 17 base) to 64.7% (11 GC in 17 base). The probes symbol, sequence, GC contents, mutation position and type were listed in Table 2.5. A 5′ end amino group modified and 3′ end TAMRA modified oligonucleotide probe of 17T was used as control probe in the experiment.

3.3.2 Fabrication of HBV Microarrays

The preparation of the slides and microarray spotting were described in Section 5.3 with the exception that the concentration of control probe was 20μM. The layout of the microarray is illustrated in Figure 2.20 (A). The double labeled control probe was spotted in duplex format.

3.3.3 Amplification of HBV DNA

Sample of HBV DNA was isolated from serum by phenol-chloroform extraction and ethanol precipitation. Segment the viral genome was amplified using

TABLE 2.5. The probe sequences, GC contents and nt postions

Probe	Probe Sequence	GC	NT Position
P1	NH_2-GAGCAGGA**A**TCGTGCAG	10	531 wide type
P2	NH_2-GAGCAGGA**C**TCGTGCAG	11	531 (T to G)
P3	NH_2-GCAGTTTC**C**GTCCGAAG	10	587 wide type
P4	NH_2-GCAGTTTC**T**GTCCGAAG	9	587(G to A)
P5	NH_2-ACATAGAG**G**TTCCTTGA	7	546 wide type
P6	NH_2-ACATAGAG**A**TTCCTTGA	6	546(C to T)
P7	NH_2-ACAAAGA**CC**T**T**TAACCT	6	1762 1764 wide type
P8	NH_2-ACAAAGA**CC**A**T**TAACCT	6	1762(A to T)
P9	NH_2-ACAAAGA**T**C**TT**TAACCT	5	1764(G to A)
P10	NH_2-ACAAAGA**T**C**A**TTAACCT	5	1762(A to T) 1764(G to A)
F	NH_2-TTTTTTTTTTTTTTTT-TAMRA		Control Sequence

Bold underline indicates the single nucleotide mutation of HBV.

duplex PCR with primers GTTGCCCGTTTGTCCTCT (forward) and GATGTTGTACAGACTTGGCC (reverse), and GGCATACTTCAAA-GACTGTG (forward) and GAAGGAAAGAAGTCAGAAGG (reverse). The PCR reactions were performed in a total volume of 25 μL containing 1 U Taq polymerase (Takara Shuzo Co. Ltd., Japan), 1×PCR buffer, 0.2 mM

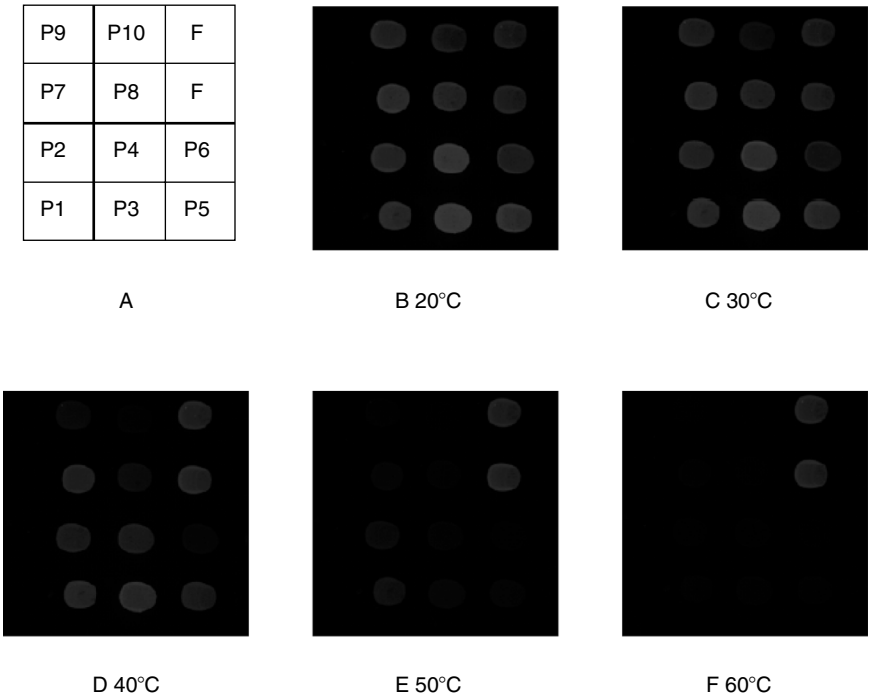

FIGURE 2.20. Probes Layout (A) and Fluorescence Image of the HBV microarray at different temperature (B)-(F).

dATP, dCTP, dGTP and 0.16 mM dTTP and 0.04mM SpectrumRed-dUTP (Vysis Co. USA), 1μl DNA template sample and 500 nM of each primer. Amplification condition consisted of an initial 10-min denaturation at 94 ˚C followed by 30 cycles of 30s of denaturing at 94 ˚C, 30 s of annealing at 52 ˚C, and 30s of extension at 72 ˚C.

3.3.4 Melting Curve Measurement of the HBV Microarray

The PCR product was applied to the HBV microarray at 20 ˚C for 10 minutes. Then the microarray was mounted on the hybridization chamber containing hybridization buffer ((10mM PBS (pH=7.0) and 1M sodium chloride). Melting experiment was carried out with the temperature increasing from 20 ˚C to 60 ˚C at a rate of 2 ˚C/min.

The fluorescence images were collected every minute by laser scanning confocal microscope. The fluorescence was excited with 568nm line of Kr-Ar ion laser and the collection was performed with the standard TRITC filter.

The fluorescence images of the microarray at 20-60 ˚C are shown in Figure 2.20 (B) to (F). The fluorescence intensity of the TAMRA labeled control probes shows no apparent change, which indicates the photobleaching during experiment is neglectable.

Figure 2.20 (B), we can see the fluorescence intensity difference between low GC content matched and mismatched probes. The fluorescence intensity of two base mismatched p10 and one base mismatched probe p8 and p9 is much lower than that of perfect matched probe p7. The perfect matched probe p5 is brighter than one base mismatched p6. There are no difference of the higher GC contents matched and mismatched probe p1, p2, p3 and p4.

When the temperature is increased to 30 ˚C, as shown in Figure 2.20 (C), the two base mismatched probe p10 is hard to see. And the fluorescence contrast between p5 and p6 is improved.

Further increase the temperature to 40 ˚C, as shown in Figure 2.20 (D), the low GC contents mismatched probes: p6 and p8, p9, p10 are hardly to see. The fluorescence intensities of higher GC content matched probe p1 and p3 are higher than those of mismatched p2 and p4, respectively.

At 50 ˚C in Figure 2.20 (E), only the highest GC content perfect matched probe p1 and fluorescence labeled control probes can be seen.

At 60 ˚C in Figure 2.20 (F), only the fluorescence labeled control probes are discernable.

The fluorescence intensity versus temperature of four location of HBV mutation is plotted in Figure 2.21. The fluorescence intensities are normalized with the average intensities of two control probes to minimize the effects of laser fluctuate and fluorescence bleaching during the continuous scanning.

The melting curve data were submitted to the web-based dissociation temperature calculation software and the returned results are listed in Table 2.6.

The single nucleotide mismatch discrimination ratios at different temperatures were calculated and shown in Figure 2.22. We can see from the Figure 2.22 and Table 2.6, the largest difference of fluorescence intensities reaches

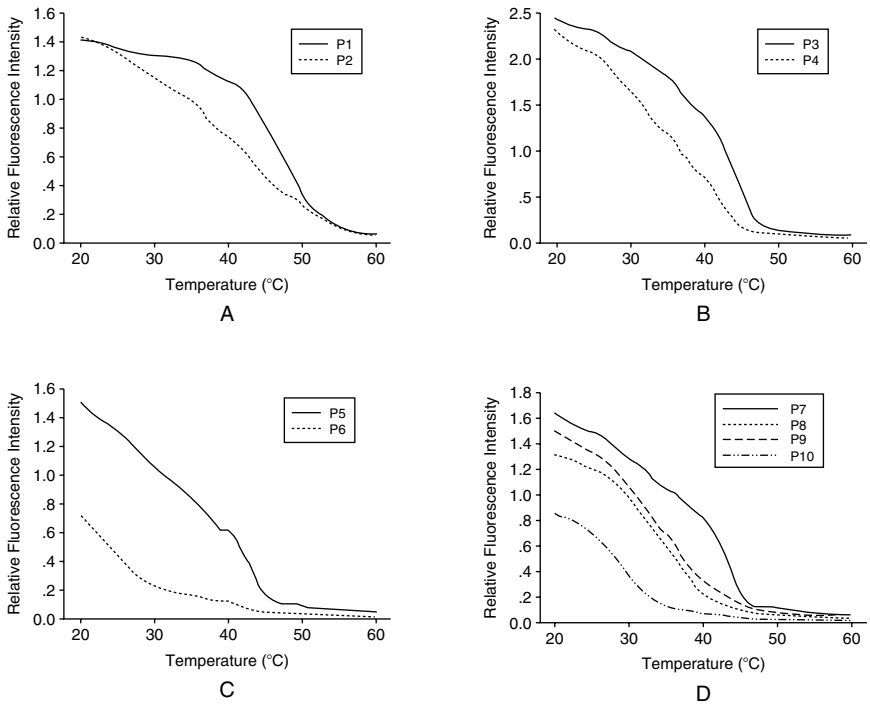

FIGURE 2.21. Fluorescence intensity versus temperature of the HBV microarray.

when the temperature is between the dissociation temperature of the perfect matched and one base mismatched duplex. The results can be further confirmed by the plot of single nucleotide mismatch discrimination ratio versus temperature in Figure 2.22. The highest discrimination ratios of p1 to p2, p3 to p4, p5 to p6, p7 to p8 and p7 to p9 are at 45 ˚C, 45 ˚C, 42 ˚C, 41 ˚C and 40 ˚C, respectively.

3.3.5 Discussion

We reported a microarray based non-equilibrium melting curve analysis method and its application in detecting HBV mutations in this section. The results indicate that the single nucleotide mismatch with a wide range of GC contents on the same microarray can be readily and reliably distinguished. With this method, the hardware requirements of microarray systems in clin-

TABLE 2.6. Dissociation temperature of each probe

P1	P2	P3	P4	P5	P6	P7	P8	P9	P10	P1
47.3	42.3	42.9	36.5	39.3	26.9	42.3	35.1	34.9	29.7	47.3

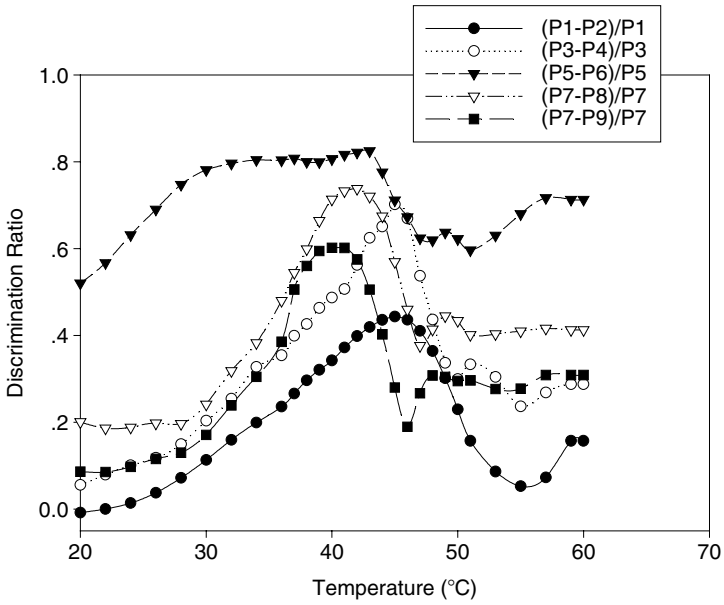

FIGURE 2.22. Single nucleotide mismatch discrimination ratio versus temperature of the HBV microarray.

ical applications were greatly decreased. The results are derived from a serial of images at different temperature instead of a single hybridization image, so even with microscope equipped with low precision temperature controller will give reliable conclusions. Moreover, this method will resolve the problem of normalization of the hybridization conditions of large number of probes in high density microarray. Several hybridization images at different temperatures will easily provide reliable sequence information of large number of different targets.

3.4 Conclusions

We investigated and compared the melting properties of oligonucleotide duplexes in solution and on microarrays. Though many publications reported the thermodynamic properties of duplex in solution with different compositions and mismatch types and positions, few data are available for duplexes on microarrays. Investigating the thermodynamic parameters and understanding the factors influencing the melting properties at the solid-liquid interface are necessary and fundamental for the application of microarray technology. Our results indicate the duplexes on microarrays show low thermal stabilities and the melting curves of them are greatly broadened and depressed by the surface effects.

One important factor effect the clinical application of microarray is the reliability of single nucleotide mismatch discrimination. Surface effects reduce the fluorescence difference between the perfect matched and single base mismatched duplexes, which makes it difficult to get reliable results from a single hybridization image. Our application of the non-equilibrium melting curve analysis method in HBV mutation detection showed great single nucleotide mismatch discrimination ability over a wide range of GC contents on the same microarray, which indicate a wide application of this method in microarray composed of probes with different length, base composition and mismatch positions. The potential of this method in detecting unbalanced alleles and mutations are under investigation.

Acknowledgements. This research work is supported by National Natural Science Foundation (project No. 60121101), the State Key Fundamental Research Scheme (973 project No.G1998051200), and the State Key High-Technology Scheme (863 project No. 2002AA2Z2004).

References

1. Lander ES. Array of hope. NAT GENET. 1999, 21S: 3-4.
2. Michael JH. DNA microarray technology: devices, systems, and applications. Annu Rev Biomed Eng, 2002, 4: 129-153.
3. Blohm DH, Guiseppi-Elie A. New developments in microarray technology. Curr Opin Biotechnol, 2001, 12: 41-47.
4. Fodor SPA, Read L, Pirrung M, Stryer L, Lu AT, and Solas D. Light-directed, spatially addressable parallel chemical synthesis. Science, 1991, 251: 767-773.
5. Fodor SPA, Rava RP, Huang XC, Pease AC, Holmes CP, Adams CL. Multiplexed biochemical assays with biological chips. Nature, 1993, 364: 555-557.
6. Okamoto T, Suzuki T, Yamamoto N. Microarray fabrication with covalent attachment of DNA using Bubble Jet technology. Nat Biotechnol, 2000, 18 (4): 438-441.
7. Xiao PF, He NY, He QG,, Zhang CX, Wang YW, Lu ZH, Xu JQ. DNA microarray synthesis by using PDMS molecular stamp (II) -Oligonucleotide on-chip synthesis using PDMS stamp. Science in China Series B-Chem., 2001, 44: 442-448.
8. Schena M, Shalon D, Davis RW, Brown PO. Quantitative monitoring of gene expression patterns with a complementary DNA microarray. Science, 1995, 270: 467-470.
9. Collins FS, Guyer MS, Chakravarti A. Variations on a theme: cataloging human DNA sequence variation. Science, 1997, 278: 1580-1581.
10. Hurles M Are 100,000 "SNPs" useless? Science, 2002, 298 (5598): U1-U1
11. Syvanen AC. Accessing genetic variation: Genotyping single nucleotide polymorphisms. Nat Rev Genet, 2002, 2 (12): 930-942.
12. Breen G. Novel and alternate SNP and genetic technologies. Psychiatr Genet. 2002,12(2):83-88.
13. Tyagi S, Kramer FR. Molecular beacons: probes that fluoresce upon hybridization. Nat Biotechnol, 1996, 14: 303-308.
14. Kostrikis LG, Tyagi S, Mhlanga MM, Ho DD, and Kramer FR Spectral genotyping of human alleles. Science, 1998, 9:1228-1229.
15. Giesendorf BA, Vet JA, Tyagi S, Mensink EJ, Trijbels FJ, and Blom HJ Molecular beacons: a new approach for semiautomated mutation analysis. Clin Chem, 1998, 44:482-486.

16. Eun AJC and Wong SM Molecular beacons: a new approach to plant virus detection. Phytopathology, 2000, 90:269-275.
17. Fortin NY, Mulchandani A, and Chen W Use of real-time polymerase chain reaction and molecular beacons for the detection of Escherichia coli O157:H7. Anal Biochem, 2001, 289:281-288.
18. Yates S, Penning M, Goudsmit J, Frantzen I, van De Weijer B, van Strijp D, and van Gemen B Quantitative detection of Hepatitis B Virus DNA by real-time nucleic acid sequence-based amplification with molecular beacon detection. J Clin Microbiol, 2001,39:3656-3665.
19. Perlette J and Tan W, Real-time monitoring of intracellular mRNA hybridization inside single living cells. Anal Chem, 2001,73:5544-5550.
20. Li JJ, Fang XH, Schuster SM, and Tan WH. Molecular beacons: a novel approach to detect protein -DNA interactions. Angew Chem Int Ed. 2000, 39: 1049-1052.
21. Tyagi S, Bratu DP, and Kramer FR, Multicolor molecular beacons for allele discrimination. Nat Biotechnol, 1998, 16: 49-53.
22. Tyagi S, Marras SAE, Kramer FR. Wavelength-shifting molecular beacons. Nat Biotechnol, 2000, 18: 1191-1196.
23. Dubertret B, Calame M, Libchaber AJ. Single-mismatch detection using gold-quenched fluorescent oligonucleotides. Nat Biotechnol, 2001,19 (4): 365-370.
24. Liu X and Tan W A fiber-optic evanescent wave DNA biosensor based on novel molecular beacons. Anal Chem. 1999, 71: 5054-5059.
25. Liu X, Farmerie W, Schuster S, Tan W. Molecular beacons for DNA biosensors with micrometer to submicrometer dimensions. Anal Biochem. 2000, 283: 56-63.
26. Brown LJ, Cummins J, Hamilton A, Brown T. Molecular beacons attached to glass beads fluoresce upon hybridisation to target DNA. Chemical Comm. 2000: 621-622.
27. Steemers FJ, Ferguson JA, and Walt DR. Screening unlabeled DNA targets with randomly ordered fiber-optic gene arrays. Nat Biotechnol. 2000, 18: 91-94.
28. Wang H., Li J, Liu HP, Liu QJ, Mei Q, Wang YJ, Zhu JJ, He NY, and Lu ZH. Label-free hybridization detection of a single nucleotide mismatch by immobilization of molecular beacons on an agarose film. Nucleic Acids Research 2002. 30:e61.
29. Bowtell D, Sambrook J, A molecular cloning manual: DNA microarrays. Gold Spring Harbor Laboratory Press. 2002, 61-100.
30. Proudnikov D, Timofeev E, Mirzabekov. Immobilization of DNA in polyacrylamide gel for the manufacture of DNA and DNA-oligonucleotide microchips. Anal Biochem. 1998, 259(1):34-41.
31. Guschin,D., G.Yershov, A.Zaslavsky, Gemmell A, Shick V, Proudnikov D, Arenkov P, Mirzabekov A.. Manual manufacturing of oligonucleotide, DNA, and protein microchips. Analytical Biochemistry. 1997, 250: 203-211.
32. Timofeev E, Kochetkova SV, Mirzabekov AD, Florentiev VL. Regioselective immobilization of short oligonucleotides to acrylic copolymer gels. Nucleic Acids Res. 1996 ,24(16):3142-3148.
33. Afanassiev,V., V.Hanemann, and S.Wolfl. Preparation of DNA and protein micro arrays on glass slides coated with an agarose film. Nucleic Acids Research. 2000, 28: E66.
34. Zivelin,A., Rosenberg,N., Peretz,H., Amit,Y., Kornbrot,N. and Seligsohn,U. Improved method for genotyping apolipoprotein E polymorphisms by a PCR-based assay simultaneously utilizing two distinct restriction enzymes. Clin. Chem., 1997, 43:1657-1659.

35. Akey JM, Shriver MD. Melting curve analysis of SNPs (McSNP): A simple gel-free low-cost approach to SNP genotyping and DNA fragment analysis. CLIN CHEM. 2000, 46 (11): 28
36. Bullock GC, Bruns DE, Haverstick DM. Hepatitis C genotype determination by melting curve analysis with a single set of fluorescence resonance energy transfer probes. CLIN CHEM. 2002, 48 (12): 2147-2154
37. Howell WM, Jobs M, Gyllensten U, et al. Dynamic allele-specific hybridization-A new method for scoring single nucleotide polymorphisms. NAT BIOTECHNOL. 1999, 17 (1): 87-88
38. Drobyshev A, Mologina N, Shik V, Pobedimskaya D, Yershov G, Mirzabekov A. Sequence analysis by hybridization with oligonucleotide microchip: identification of beta-thalassemia mutations. Gene. 1997, 25, 188(1): 45-52.
39. Fotin AV, Drobyshev AL, Proudnikov DY, Perov AN, Mirzabekov AD. Parallel thermodynamic analysis of duplexes on oligodeoxyribonucleotide microchips. Nucleic Acids Res. 1998, 15; 26(6): 1515-21.
40. Gilles PN, Wu DJ, Foster CB, et al. Single nucleotide polymorphic discrimination by an electronic dot blot assay on semiconductor microchips. Nat Biotechnol. 1999, 17(4): 365-70.
41. Urakawa H, Noble PA, El Fantroussi S, Kelly JJ, Stahl DA. Single-base-pair discrimination of terminal mismatches by using oligonucleotide microarrays and neural network analyses. Appl Environ Microbiol. 2002,68(1):235-44
42. Hou,J.L., Wang,Z.H., Cheng, J.J. et al. Prevalence of naturally occurring surface gene variants of hepatitis B virus in nonimmunized surface antigen-negative Chinese carriers. Hepatology, 2001, 34: 1027-1034.
43. Chen,W.N. and Oon,C.J. Human hepatitis B virus mutants: significance of molecular changes. Febs Letters, 1999, 453: 237-242.

http://www.springer.com/978-0-387-25568-2

Frontiers in Biochip Technology
Xing, W.-L.; Cheng, J. (Eds.)
2006, X, 358 p., Hardcover
ISBN: 978-0-387-25568-2